2015•2016
FACULTEIT INDUSTRIËLE INGENIEURSWETENSCHAPPEN
master in de industriële wetenschappen: energie

Masterproef

Detection and acceleration of potential induced degradation on silicon photovoltaic modules

Promotor :
Prof. dr. ir. Michael DAENEN

Promotor :
ing. JORNE CAROLUS

Jordy Coppieters

Scriptie ingediend tot het behalen van de graad van master in de industriële wetenschappen: energie

Gezamenlijke opleiding Universiteit Hasselt en KU Leuven

KU LEUVEN | universiteit hasselt

KU LEUVEN | universiteit hasselt

2015•2016

Faculteit Industriële ingenieurswetenschappen

master in de industriële wetenschappen: energie

Masterproef

Detection and acceleration of potential induced degradation on silicon photovoltaic modules

Promotor :
Prof. dr. ir. Michael DAENEN

Promotor :
ing. JORNE CAROLUS

Jordy Coppieters

Scriptie ingediend tot het behalen van de graad van master in de industriële wetenschappen: energie

universiteit hasselt | KU LEUVEN

Acknowledgements

The realization of this master's thesis was an interesting and educational experience and it fulfilled all the expectations I envisioned. With the support and criticism of others, this thesis has been brought to a concluding end. Therefore I would like to say my gratitude to the people who invested their time into this master's thesis.

Firstly I would like to show my deepest appreciation to my supervisor Prof. dr. ir. Michaël Daenen and co-supervisor ing. Jorne Carolus. They provided me with their knowledge and guidance when I encountered a problem.

Additionally, I would like to thank the co-workers at the Institute for Materials Research (IMO) and Hasselt University; ing. Jan Mertens and Mr. Lieven De Winter for their critical assessment and their technical knowledge, Mr. Johnny Baccus for assisting me in choosing the right pneumatic components and Mr. Johan Soogen for his practical skills in creating mechanical off the shelf components.

I would also like to thank my family and friends for their support throughout my academic career.

Jordy Coppieters
June 2016

Table of Contents

List of tables

List of figures

List of abbreviations

AM	Air Mass
ARC	Anti-Reflective Coating
BDE	Biomedical Device Engineering
DH	Damp Heat
EL	Electroluminescence
EMAP	Engineering Materials and Applications
ESE	Energy Systems Engineering
EVA	Ethylene-Vinyl Acetate
FL	UV Fluorescence
FME	Function Materials Engineering
GPIB	General Purpose Interface Bus
IMO	Institute for Materials Research
IR	Infrared
LIT	Lock-In Thermography
MPP	Maximum Power Point
PID	Potential Induced Degradation
PV	Photovoltaic
RH	Relative Humidity
SMU	Source Measuring Unit
UV	UltraViolet
VI	Virtual Instruments

Abstract

Research group Energy System Engineering (ESE), led by Prof. dr. ir. Michael Daenen, is established in the Institute for Materials Research (IMO). ESE investigates the reliability of photovoltaic (PV) modules. Potential Induced Degradation (PID) is a common degradation of industrial PV installations. The main goal of this thesis was the realization of a test setup in order to accelerate PID on silicon PV modules.

There are several methods to determine PID, but two methods were chosen for this thesis. The first method is through an electroluminescence (EL) image. This is taken by a modified webcam. The images are edited in LabVIEW by a self-written program. The program provides a greater contrast between the different parts of a PV module. The second way is by measuring the efficiency of the PV module. This can achieved by measuring the current voltage (IV) curve of the PV module. According to the standard, this measurement has to be carried out under standard test conditions. This was not possible because the solar simulator needs to warm up. This allows the PV module to increase in temperature, which will result in a decrease in efficiency. A shutter was placed in front of the solar simulator in order to avoid the raise of temperature of the sample under test.

The results show that accelerating PID can be achieved. By measuring the IV curves, it can be concluded that the efficiency of the PV module decreased by 34 % after a PID test. After curing the PV module, the efficiency increased again by 35,4 %, which is an increase of initial efficiency of 1,4 %. The increase could be caused by a lower module temperature during IV measurements.

Samenvatting

Onderzoeksgroep Energy System Engineering (ESE), onder leiding van Prof. dr. ir. Michaël Daenen, is gevestigd in het instituut voor materiaalonderzoek (IMO). ESE doet onderzoek naar de betrouwbaarheid van fotovoltaïsche (PV) modules. Potential Induced Degradation (PID) is een veelvoorkomende degradatie bij industriële installaties van PV modules. Het hoofddoel van deze masterthesis was de realisatie van een testopstelling om PID te versnellen bij silicium PV panelen.

Er zijn verschillende manieren om PID vast te stellen, maar in deze scriptie is er gekozen om 2 manieren uit te werken. De eerste manier is via een elektroluminescentie (EL) foto. Deze wordt genomen door een aangepaste webcam. De foto's worden bewerkt in LabVIEW door een zelf geschreven programma. De software zorgt voor een groter contrast tussen verschillende delen van de PV module. De tweede manier is door de efficiëntie van de PV module te meten. Deze kan men uit een stroom-spanning (IV) curve halen. Volgens de norm moet deze meting uitgevoerd worden onder standaard test condities. Dit was niet mogelijk doordat de zonnesimulator moet opwarmen. Dit zorgt ervoor dat de PV module zal opwarmen en de efficiëntie ervan zal dalen. Een shutter werd voor de zonnesimulator geplaatst om deze opwarming te vermijden.

De resultaten tonen aan dat PID versnelt opgewekt kon worden. Door IV curves te meten kan er geconcludeerd worden dat na de PID testen de efficiëntie van de PV module gedaald was met 34 %. Na het *curen* van de PV module was de efficiëntie gestegen met 35,4 %, dit was 1,4 % hoger dan de initiële efficiëntie voor de PID test.

Chapter 1 Introduction

1.1 Situation

This master's thesis is conducted at the Institute for Materials Research in MicroElectronics, which is a local division of the Institute for Materials Research (IMO) of Hasselt University. The division Engineering Materials and Applications (EMAP) is striving to further develop fundamental research into industrially viable applications. Within EMAP there are three divisions: Energy Systems Engineering (ESE), Biomedical Device Engineering (BDE) and Functional Materials Engineering (FME). ESE does reliability testing on PV modules and how the knowledge of fundamental research can be applied to improve the reliability of the PV modules. This happens from cell level up to a complete installation. This master's thesis focuses on one of ESE's research topics: Accelerating a degradation mechanism caused by a high potential difference.

1.2 Problem description

ESE is a new research group which is fully engaged in expanding the laboratory where PV modules are being tested. Therefore ESE wanted a setup to perform degradation tests and measure this degradation on PV solar cells. More specific the degradation of PV modules caused by high voltages between the PV cell and the PV module's frame. This kind of degradation is called potential induced degradation (PID).

PID occurs when a large number of PV modules are connected in series. This means that the cells near the end of the string have a large potential difference (up to 1000 V) between the cell and the grounded frame of the PV module. The electric field created by this high potential difference will cause a leakage current of electrons to flow. This electron leakage current will drive positive sodium (Na) ion mobility within the module between the cell and the frame, through the glass and EVA layer. Na-ions, which are present in the soda lime glass, will migrate into the EVA encapsulate, which causes the EVA to have more charge carriers. Because of the increase of charge carriers in the EVA, the leakage current will increase and therefore, more ions will be conducted. Na-ions will eventually reach the cell surface and locally shunt the semi-conductor. The increase of leakage current and local shunting will lead to loss of power of up to 40% [1, pp. 316–318], [2, p. 2].

At present, various solutions for PID are available. On a cellular level the materials used and the thickness of the anti-reflective coating (ARC) layer can be adjusted during the manufacturing process [3, p. 1]. On a modular level, the encapsulate material or the composition of EVA can be changed to reduce the leakage current. On a system level, an inverter can be used to change the grounding topology or an PID curing device can be used that sends a positive voltage during the night. Therefore affected PV modules will be cured during the night and can work at their highest efficiency. [2, pp. 3–4].

Large solar farms, that have up to 1000 V strings, often are equipped with susceptible PV modules. Therefore a large amount of, otherwise, usable energy is lost, which will elongate the payback period.

1.3 Goal

The main goal of this master's thesis is split up into 3 parts: First of all is to create a setup that is able to accelerate the degradation process on a single cell module. A Second requirement is to measure the presence of PID in the degraded cell module. The last part is that the degradation also has to be able to be cured. During testing the sensitivity for PID degradation of the test setup has to be determined.

1.4 Methodology

At first a literature study has been done to gain knowledge about the working of a PV cell and which type of degradations will impact the efficiency from a cell level up to a PV system. Information was collected on the causes of the degradation, what impact this degradation has on the PV system, how to accelerate the degradation and what standards exist for degradation and measurement setups.

It is necessary to have equipment to create a test setup to test the resilience of the different layers of a PV cell against PID. First of all, a high-voltage source is needed that is able to apply a voltage of at least -1000 V according to [4, p. 5] in order to stress PID. Second of all, a source measuring unit (SMU) is needed that can dissipate the power output of a cell. This SMU is used to measure the IV curve, a commonly used method to detect PID. Third of all, a climate chamber or an oven is required, because it is necessary that the temperature can be controlled during stress testing and measuring. Depending on the type of stress test the relative humidity needs to be controlled as well.. Fourth of all, a solar simulator is required which is able to illuminate the PV module with an intensity of 1000 W/m² [5, p. 777] with a light spectrum that is similar to the sun (AM 1.5). As last, we want to a make an electroluminescence (EL) image to visually detect whether and where the cell is degraded with PID. This will be achieved with a modified webcam, in which the IR-filter has been replaced by a visual light filter. The methods of measuring and degrading are done according to the draft version of the IEC 62804 standard. In order to log the data and process the images we need dedicated software. For this purpose, LabVIEW is used in to create the dedicated software.

Chapter 2 Literature review

2.1 PV system

A PV system can be characterized on 3 different levels. First of all on a cell level. Second of all on a module level. A module consist out of multiple cells connected in cell string laminated with an encapsulate with at least one glass side . At last on a system level. A system is multiple modules connected with each other through to an inverter which sends the generated power to the electricity grid.

2.1.1 Cell level

The most commonly used semiconductor material for PV cells is silicon (Si). A semiconductor is made up from individual Si-atoms. Si-atoms have 14 electrons of which 4 electrons are on the outer level. Because Si has 4 electrons on the outer energy level, all electrons surrounding each atom will form a covalent bond. A covalent bond is where two atoms share a single electron. Therefore a Si-atom will receive 4 electrons shared by the surrounding Si-atoms as can be seen in Figure 2-1. A PN junction needs to be made to be able to generate power [6].

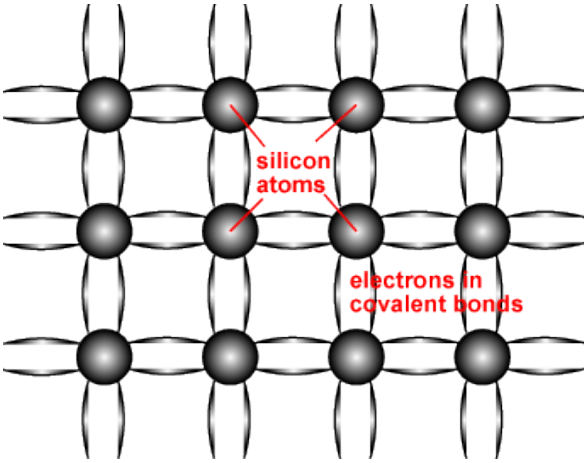

FIGURE 2-1: COVALENT BONDS IN A SILICON CRYSTAL. EACH LINE REPRESENTS AN ELECTRON BEING SHARED BETWEEN TWO ATOMS [6].

In order to create an n-type or p-type semiconductor, the balance of electrons and holes need to be shifted. This is achieved by doping the Si-crystal with other atoms. Atoms with one more electron than Si are used to create the n-type semiconductor. When this atom bonds with Si-atoms the atom roster will get 1 extra electron, which is negative. Atoms with 1 less electron than Si are used to create the p-type semiconductor. This will result in one extra hole, which provide a positive charge[6]. A representation of N-type and P-type semiconductors are show in Figure 2-2.

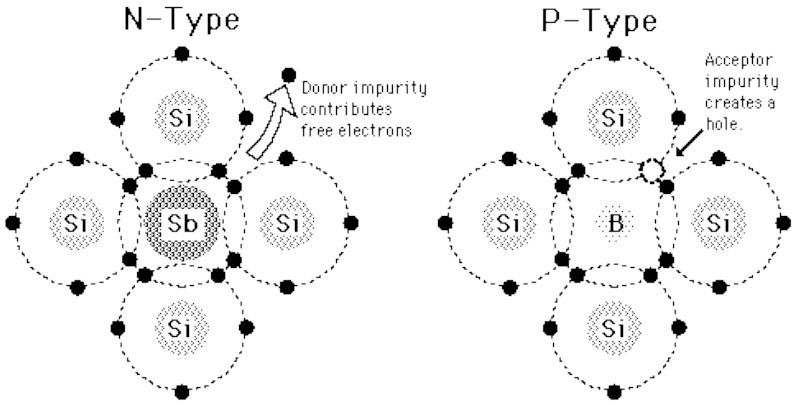

FIGURE 2-2: REPRESENTATION OF A N-TYPE AND P-TYPE SEMICONDUCTORS. THE N-TYPE IS MADE DOPING ANTIMONY IN THE SEMICONDUCTOR, BUT PHOSPHOR CAN ALSO BE USED. THE P-TYPE IS MADE BY DOPING BORON IN THE SEMICONDUCTOR [7].

A PV cell, as shown in Figure 2-3, is built out of an PN junction, which is a n- and p-type Si-semiconductor put together. According to [6], two key processes are involved to generate a current, known as the "light-generated current". First, the absorption of incident photons will create an electron-hole pair. The creation of an electron-hole pair only happens when the incident photon has energy greater than that of the band gap. Electrons and holes are meta-stable and will only exist for a length of time before they recombine. If they recombine before going through the circuit, so at the PN junction, the light-generated electron-hole pair is lost and no power can be generated.

Second, the PN-junction prevents recombination by spatially separating the electron and the hole. They are separated because of the electric field existing at the PN-junction caused by bringing a n- and p-type semiconductor together. If the minority carrier reaches the PN-junction, it will be swept across the junction by the electric field at the junction, where it becomes a majority carrier. The light generated carrier will flow through the external circuit if the anode and cathode of the solar cell are connected together. The amount of energy a photon can transfer is determent by Equation 2-1 [6], [8, p. 757].

$$E_{ph} = h * f \qquad (2\text{-}1)$$

h is Planck's constant and f is the frequency of the photon radiation. To complete the PV cell, conductive strips are soldered on the front as well as on the back of the cell, therefore the electron can move from the positive side, through a load, to the negative side . Then, the front of the cell is coated with an anti-reflective coating (ARC) to improve the efficiency. The ARC redirects light that is reflected by the cell surface, back to the cell. A close-up of a laminated PV cell can be seen at Figure 2-3 [6], [8, p. 757].

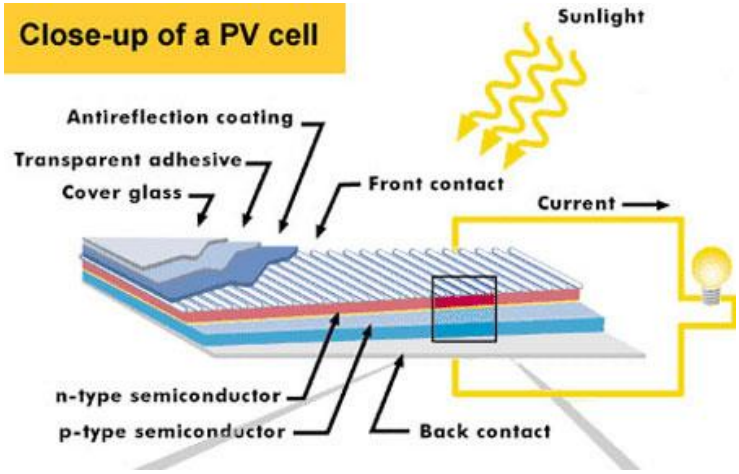

FIGURE 2-3: COMPOSITION OF A ENCAPSULATED PV CELL AND HOW A CURRENT WILL FLOW FROM THE FRONT CONTACT TO THE BACK CONTACT [9].

2.1.2 Module level

A PV module consists out of PV cells connected in series or parallel, called string. Bypass diodes are connected across each string, with the intention to protect the cells against mismatching. These connected cells are then encapsulated in a clear polymer and it is made sure that two connection are reachable on the outside in order to connect the module. Different polymers can be used but ethylene-vinyl acetate (EVA) is the most common material, Polyolefin is another polymer used. The back of the module incorporates a layer to protect the PV cells and electrical components, called the back sheet and can be made out of tedlar. On the front soda lime glass is placed. Sodium, a charge carrier, is present in the soda-lime glass to lower the melting temperature during the manufacturing process. Then a metal frame is placed over the edges keeping all the layers together and protecting then against moisture and dust. As last a junction box is placed on the back of the module, this allows the module to be connected to other modules or an inverter [6], [10].

2.1.3 System level

A system consists out of individual PV modules connected in series, these are called strings. The strings are then parallel connected to an inverter, which will convert the direct current into alternating current so that the PV system can be connected to the grid. Another function of the inverter can be to track the maximum power point of the PV system to get the maximum possible power from the PV arrays. This is done by sampling the output of the modules and determining a resistance load to obtain maximum power for any given environmental conditions [11], [12].

More than 236.527 system installed in Flanders have a power capacity of less than ten kW. These are all private PV systems, typically build on the roofs of houses. Industrial installations have a capacity of more than ten kW and there are 5.903 in operation in Flanders [13].

2.2 Degradations by cause

The definition of degradations:

"Degradation is the gradual deterioration of the characteristics of a component or of a system which may affect its ability to operate. Manufacturers consider a PV module degraded when its power reaches a level below 80 % of its initial power" [14, p. 142].

2.2.1 Temperature

2.2.1.1 Hot spots

A hot spot can damage an element of the module. Causes of a hot spot are partial shadowing of a cell, cells mismatch or failure of the interconnect ribbons between cells. The voltage of a defective PV cell is reversed and becomes equal and opposite to the voltage of the other cells in series. This defective cell will become a load for other cells and thus a place of a high thermal dissipation. Bypass diodes will ensure that other strings of cells will not contribute to the load of a defective cell as shown on Figure 2-4 [14, p. 145].

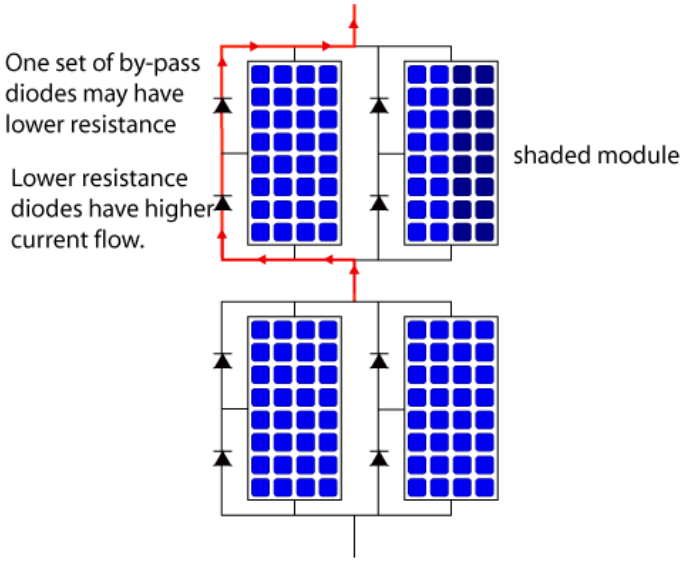

FIGURE 2-4: FUNCTION OF A BYPASS DIODE IN A PARALLEL STRING OF PV MODULES CONNECTED IN SERIES, WHERE ONE OF THE MODULE HAS SHADED CELLS [6].

Hot spots can be detected by an IR-image of the defective modules ,where the defective cells can be noticed as they have a higher temperature than the surrounding cells. It can also be noticed by a hot spot on the bypass diode because the bypass diode will be conducting the current of the other strings. It is possible to accelerate this degradations with a hot-spot endurance test [15, pp. 8–9]. According to the IEC 61215 a hot-spot endurance test is done by heating up certain parts of the PV module to see if any failures will occur within the module.

2.2.1.2 Bubbles

A bubble usually appears due to a chemical reaction where gasses are released. The lack of adherence of the EVA affects only a small area and is combined with the blowing of areas where this adherence has been lost. When it occurs at the backside of the PV module, it will become more difficult for the cells to dissipate their heat. Therefore, overheating them and subsequently reducing the lifetime of a cell. A bubble on the front side will make the heat dissipation more difficult and the reflection of the sunlight will increase.

In an early stage, a bubble can only be detected by using IR-techniques, as it is not noticeable through visual inspection, but rather causes a temperature change. In a later stage, a bubble can be visible by the naked eye because of a deformation in the module [14, pp. 145–146], [16, p. 2270].

2.2.2 Humidity

2.2.2.1 Corrosion

Moisture entering the module will cause corrosion. The corrosion will oxidize the metallic connections, which will cause a performance loss due to an increase in leakage current. Corrosion will lead to a degradation of the adhesion between the cells and the encapsulate. Moisture inside the housing of the module will increase the electrical conductivity of the material. Corrosion can be detected by looking at the module itself [14, p. 143]. An example is given in Figure 2-5.

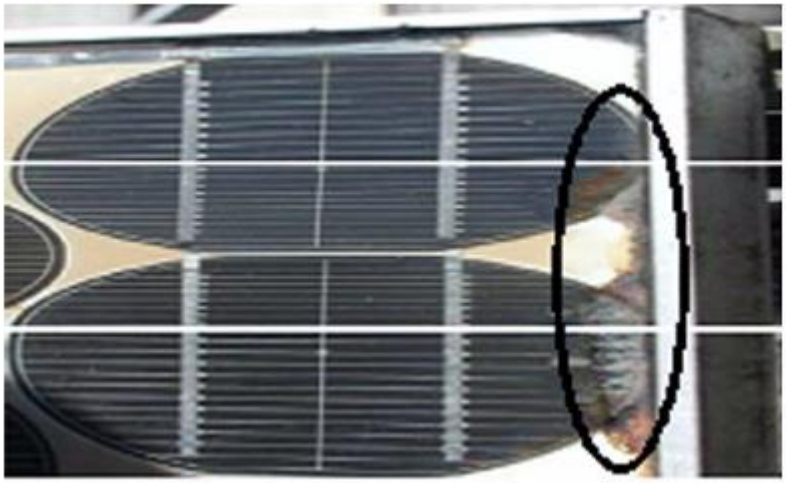

FIGURE 2-5: PV MODULE AFFECTED BY CORROSION [14].

There are three tests that can be used to accelerate corrosion according to IEC 61215. First of all, a standard test called the Damp-Heat test, DH1000. The purpose is to determine how long the module can withstand exposure to penetration of humidity, over a long period, by applying 85 °C ± 2 °C with a relative humidity of 85 % ± 5 % for the duration of 1000 hours [15, p. 10].

A second test is the Humidity-freeze test. This test will determine the module's ability to withstand the effects of high temperatures combined with humidity, followed by extremely low, sub-zero, temperatures [15, pp. 10–11].

A third test is the Wet leakage current test. This test evaluates the insulation of the module against moisture penetration under wet operating conditions, such as rain, fog, dew, melted snow, etc., in order to avoid corrosion, ground fault and thus electric shock hazard [15].

2.2.2.2 Delamination

Delamination is loss of adhesion between the encapsulating polymer and the cells , between the encapsulating polymer and the front glass or between the encapsulate and the back sheet. This causes three effects: First, the increase of the light reflection, the increase of water penetration into the module structure and an increase of cell temperature caused by the isolation caused by the thermal properties of air. Delamination is more frequent in hot and humid climates and it starts at the edges of the module. Second, it causes moisture penetration in the module, which causes various chemical and physical degradations such as metal corrosion of the module structure [14]. Delamination is visible by the naked eye and shows as white spots on the module, as shown in Figure 2-6.

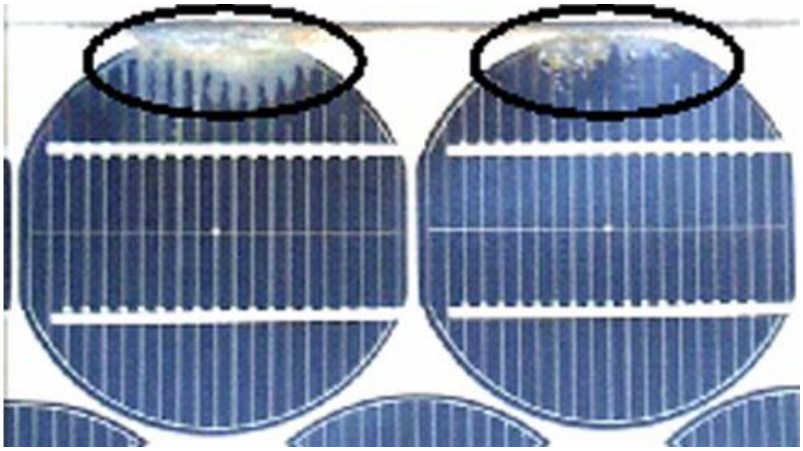

FIGURE 2-6: PV MODULE WITH DELAMINATION [14].

There are two tests that can be used to accelerate delamination; the abovementioned damp heat test and the humidity freeze test.

2.2.3 Radiation

2.2.3.1 Discoloration

Discoloration is usually the result of the encapsulate, EVA or another adhesive material between the glass and the PV cells, degrading. Module discoloration is a change in colour of the material, which turns yellow and sometimes even brown. It lowers the transmittance of light reaching PV cells and therefore the power generated by the module is reduced [14]. The discoloration is caused when the encapsulate is exposed to Ultra Violet (UV)-light. The process is accelerated when the cell is hot (overheating) or when an interconnect fails. The discoloration is visible to the eye as a yellow and sometimes brown discoloration, as seen on Figure 2-7 [17].

FIGURE 2-7: DISCOLORATION OF PV MODULE [14].

An irradiance test called UV preconditioning is used to identify materials that are susceptible to UV degradation. According to IEC 61215, the module needs to be subjected to a total UV irradiance of 15 kWh/m² in the UVA (320 nm – 400 nm) + UVB regions (280 nm -320 nm), with at least 5 kWh/m² in the UVB region. While the module will be kept at a temperature of 60 °C ± 5 °C [15, p. 9].

2.2.4 Mechanical

2.2.4.1 Breakages and micro-cracks

In recent years the thickness of silicon PV cells have decreased from 300 μm to less than 200 μm and in some cases even to less than 100 μm. In addition to the reduction in thickness of PV cells, the cell surface has increased to 210 mm by 210 mm. This makes the PV cells more fragile and more susceptible to breakage during handling [14, pp. 144–145].

Glass and PV cell breakage can occur during installation, maintenance and especially during the transportation of modules to their installation sites. These modules may keep functioning correctly. However, the risk of an electrical shock and moisture infiltration increases [14, p. 144]. Figure 2-8 shows an EL image of a PV cell with cracks. Micro-cracks in PV cells can reduce the power generation depending on which mode of crack is present.

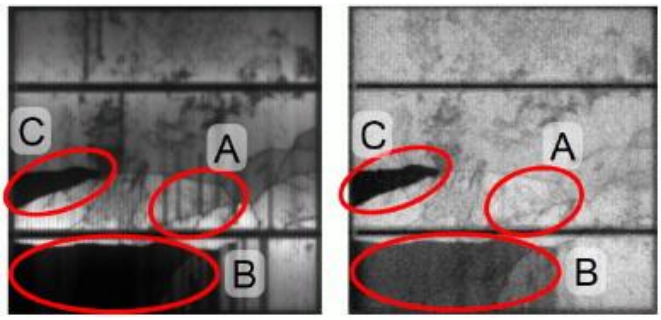

FIGURE 2-8: ELECTROLUMINESCENT IMAGES OF THE SAME PV CELL WITH CRACKS MODE A,B AND C. LEFT IMAGE IS TAKEN AT SHORT CIRCUIT CURRENT (I_{SC}) AND RIGHT IMAGE IS TAKEN AT 10% I_{SC} [18].

An A-mode crack is a crack that is not completely black at Isc and $1/10_x$ Isc. B-mode crack is a crack that is completely black at Isc but will light up at $1/10_x$ Isc. This means that this part of the cell is still connected to the rest of the cell. A C-mode crack is a crack that is dark at Isc and at $1/10_x$ Isc. Therefore this part of the cell is completely disconnected from the rest of the cell. If all cells have A-mode cracks, a power loss of ±2,5 % is estimated. With B-mode cracks there is about a maximum loss of 10 % observed. C-mode cracks indicate that this part does not contribute to the total power generation of the PV cell [18].Micro-cracks can be detected by electroluminescence and breakages in the front glass are visible to the eye [19].

The mechanical test named 'Robustness of Terminations' is used to determine the robustness of the module's terminations, which can be wires, flying leads or screws. The modules will undergo a stress test that will simulate the mechanical stress during assembly and handling [15, p. 11].

2.2.4.2 Disconnected cell and interconnect ribbons

Weakened cells or string interconnect ribbons can break. Especially the ribbon kink between the cells is prone for fatigue breakage. This fatigue can be caused by several reasons. The first reason is poor soldering in the PV module production process. During the fabrication of the ribbon a kink may form between the cells, mechanically weakens the cell interconnect ribbon, this is caused by a too intense deformation. The distance between the cells promotes cell interconnect breakages, because the distance between cells needs to be as narrow as possible to generated as much power as possible. Furthermore, physical stress during the transportation of the PV module, thermal cycles, and/or hot spot by partial cell shading during long-term PV module operation can cause disconnects [19, p. 82].

In an early stage, it will show on an EL image, as shown in Figure 2-9, as half or a whole cell is not lighting up.

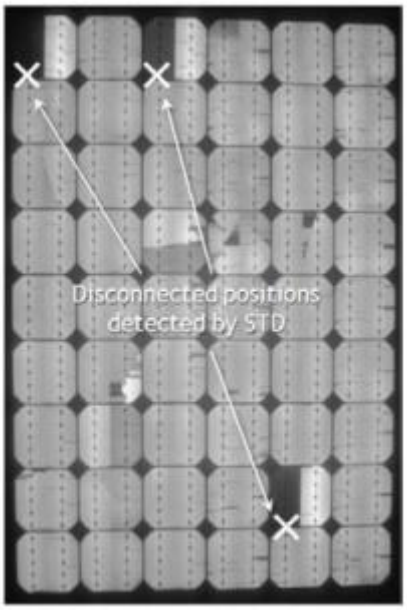

FIGURE 2-9: EL IMAGE WITH DISCONNECTED CELL INTERCONNECTIONS [19].

An infra-red imaging, as shown in Figure 2-10, shows half of the cell being warmer than the other half of the cell and that there is a hot spot on the location of a disconnected interconnect ribbon.

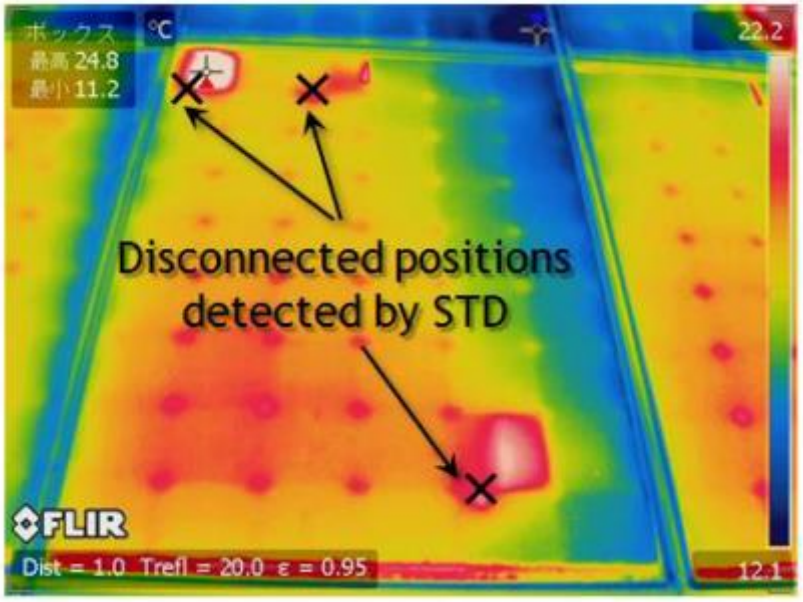

FIGURE 2-10: IR IMAGE OF A MODULE WITH DISCONNECTED CELL INTERCONNECTIONS FOUND IN THE FIELD [19].

Disconnects are also notable in a IV characteristic curve, because one disconnection can results in 35% power loss [19, p. 82]. At a later stage it can be noticed by sight. The front glass can break and burn marks on the back plate can be seen because of the temperature increase.

With a hot-spot endurance test, the PV module can be tested for this degradation [15, pp. 8–9]. According to the IEC 61215 a hot-spot endurance test is done by heating up certain parts of the PV module to see if any failures will occur within the module.

2.2.4.3 Snail tracks

A snail track is a grey/black discoloration of the silver paste of the front connectors and is visible to the human eye, as shown in Figure 2-11. This discoloration occurs at the edges of the PV cell and along cell cracks. The discoloration itself does not lead to measurable power loss. However the snail tracks make cell cracks in the solar cell visible and the disconnected cracked cells do not contribute to the overall generated power which can reduce the efficiency of the PV module. These cracks can be made more visible by using EL imaging. Modules with snail tracks show a tendency to have a higher leakage current [19, pp. 67–70].

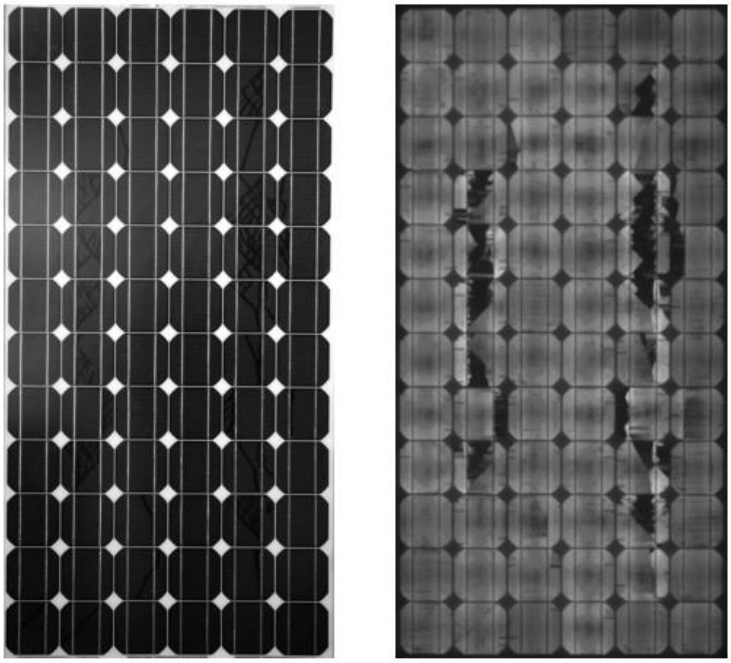

FIGURE 2-11: LEFT: SNAIL TRACKS. RIGHT: EL IMAGE OF THE SAME PV MODULE [19].

The discolorations can be hard to see with the eye. But the cracks causing the tracks can be seen by electroluminescence [19, p. 67]. [20] suggests a combination of the mechanical load, UV and humidity freeze test can accelerate the formation of snail tracks.

2.2.5 High-voltage degradation

2.2.5.1 Potential Induced Degradation (PID)

PV modules are connected with each other in series to increase the voltage of the system. Therefore the voltage can reach several hundred volts. The metallic structures of the PV modules are grounded in order to protect people against electrical shocks. It is possible that electrons escape from the PV cell through different paths, as show in Figure 2-12 [21].

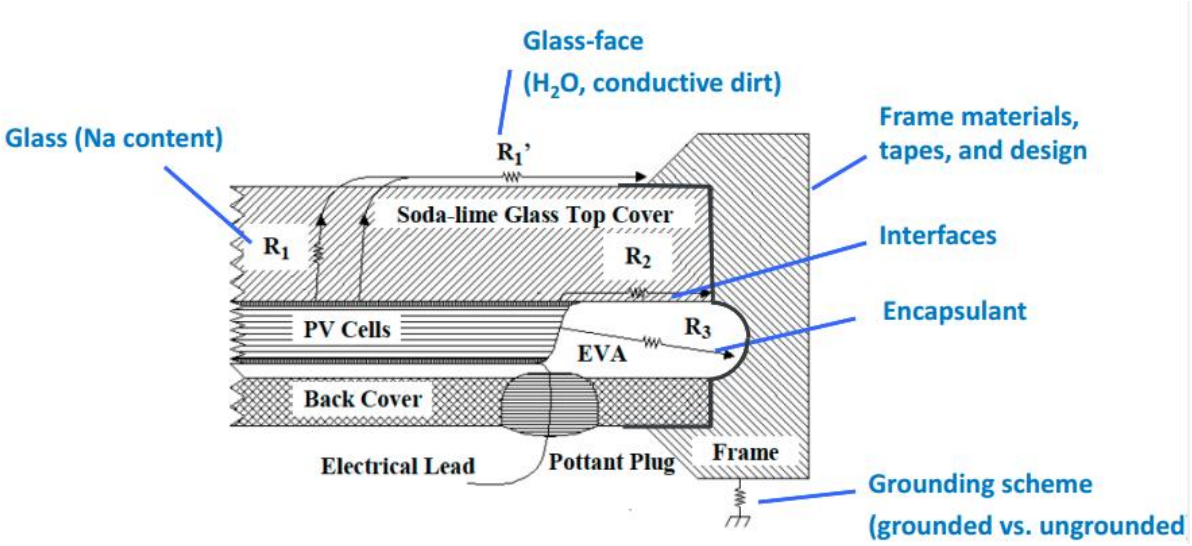

FIGURE 2-12: LEAKAGE PATHS FROM THE PV CELL TO THE MODULE FRAME [22].

This happens because of the large potential difference between the PV cells and their structure, creating a leakage current. If the current flows from the cell, through the glass, to the frame, positive ions will bond from the front glass. From this phenomenon subsists a polarization that may degrade the electrical characteristics of the PV cells. A chemical degradation is also observed, where the positive Na-ions are migrating through the encapsulate to the PV cell and creating local shunting of the PV cell. This will cause an increase of power loss on the cell level. The leakage current will increases with an increase of humidity. This is because humidity will lower the resistance of the path from the glass-face to the frame [21], [23].

PID can be detected by using different methods. One of is using thermography on an operating module array under illumination. PID will create shunting inside the PV cell. This means that the cell will have a lower output and this can be measured with an IV curve. Because of the internal shunting PID can also be detected by EL imaging. The area that has been affected by PID will show up as a dark area on the image.

Another method is by taken high resolution EL images. The locations where the cell is shunted will show up as a darker spots on the image. This is caused by the higher loss of power, thus less light will be emitted from that area. Lastly measuring the IV curve will give an indication if the PV cell suffers from PID. This is clear by looking at the angle of the tangent at I_{sc},as shown in Figure 2-13 [23], [24].

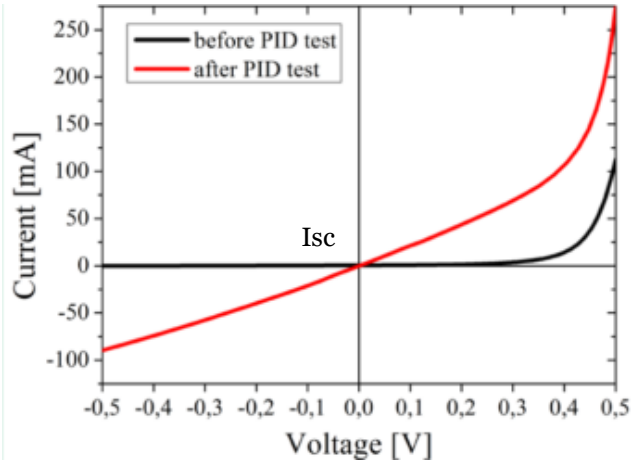

FIGURE 2-13: DARK IV CURVE, OF A 4 BY 4 CM² SOLAR CELL, BEFORE AND AFTER A PID TEST.

A conductive foil can be laid on top of the solar cell. Where the foil is grounded and a differential voltage of -1000 V is set between the cell and the foil. This is done at 25 °C for 168 h [4]. To test different encapsulates, a sandwich test setup can be used. With this method a modules is made without melting the encapsulate, so the cell is sandwiched between 2 EVA & 2 glass sheets where a conducting foil is set on the top half [21]. Another way to accelerate PID-degradation is to put a PV modules in a climate chamber at the maximum module voltage, 60°C and 85% RH for 96h and where the frame of the modules is grounded. During testing a leakage current of pA to µA can flow from the cell to the frame [25], [26, pp. 174–177].

A comparison has been done between these 2 methods and concluded that in a Damp Heat test the leakage current was 4-4.5 times higher than with the foil method. A PV module will be declared PID-resistant when the power loss is less than 5 % or if there is no evidence of any major defect [2].

2.3 Dynamic mechanical load test

The dynamic mechanical load test is used to simulate wind loads on a free standing PV module. As air flows against the module, the flow is separated and therefore resulting in a movement of the PV module[27]. This will fatigue the copper interconnect ribbons. To stress the solder bonds as well, a high temperature should be applied to the module during the mechanical test [28].

2.4 Detection methods

2.4.1 Thermography

2.4.1.1 Thermography under steady state conditions

Thermography is a fast, non-destructive detection technique for diagnosing thermal and some electrical failures. The measurements can be performed during normal operation for individual PV modules and large-scale systems. It is necessary that the measurements are done under steady state conditions of the PV module(s) [19].

For measurements outside, an uncooled portable IR-camera that can detect wavelengths between 8.000 – 14.000 nm is sufficient. Outdoor thermography should be performed on a sunny, cloudless day, with a minimal irradiation of 700 W/m² [19].

During measurements in the dark, an external current (comparable to I_{sc}) is supplied in the forward direction. To reduce false conclusions the operator should be aware of reflections (from buildings, clouds, and self-radiation) and the view angle should be set as close as possible to 90 ° but not less than 60 °. Measurements from the back sheet side are more accurate than from the glass side. This is because the glass blocks out most of the IR light and will diffuse the heat more because of the thickness of the glass layer, in contrast the back sheet layer is much thinner than the glass layer. Therefore the temperature gets less diffused [19].

2.4.1.2 Pulse thermography

With pulse thermography, the module is heated by flashing one or more simultaneous triggered powerful lights to generate a dynamic heat flux in the PV module. The pulse duration should not be longer than a few milliseconds to avoid blurry images. The lights are placed in front of the module and the intensity should be enough to instantaneously raise the surface temperature homogeneously by 1 K to 5 K. The recorded changes in surface-temperature are evaluated after applying a Fourier transformation, in the frequency domain, to the signals. Changing the frequency values will change the penetration depth of the heat dissipation [19].

2.4.1.3 Lock-in thermography

Lock-in thermography (LIT) is a non-destructive test method where the sample is excited and detected at a controlled frequency. This causes an enhancement of the signal to noise ratio and therefore, weak heat sources can be detected. For LIT a cooled IR-camera with a range from 2000 nm – 5000 nm or an uncooled IR-camera with a range from 8000 nm – 14000 Nm can be used. Thermal differences of around 10 µK can be made visible [19].

The excitation of a PV cell or module can be done electrically (Dark LIT) or optically with a light source (Illuminated LIT). With illuminated LIT, the measurements can be done completely contactless. For a Dark LIT the frequency of the electrical signal should be chosen which allows the heat wave to flow through the packaging materials in one cycle. Then the lock-in frequency is optimized for the highest image resolution. A good starting lock-in frequency is ~0,12 Hz when viewing from the back sheet and 0,01 Hz when viewing from the front glass. With increasing period counts the defects will become clearer in the image. With increased frequency the heat affected zone is reduced, thus enabling the determination of the exact position of the heat source [19].

2.4.2 Electroluminescence imaging

A PV cell has a PN-junction like a LED. When a current is applied to the PN-junction an electron will recombine with the holes existing in the p-type. During this recombination the electron will move from the conduction band to the valence band, thereby the excess energy gets dissipated in the form of heat and light. Thus when applying a current trough the cell, the cell will emit light. The light emitted will be at a wavelength of 1150 nm because the PN-junction is made from Silicon. This light is not visible to the naked eye as it is in the near-infrared area An Indium Gallium Arsenide (InGaAs) detector can be used to detect the light emitted at 1150 nm, as shown in Figure 2-14[19, pp. 41–46].

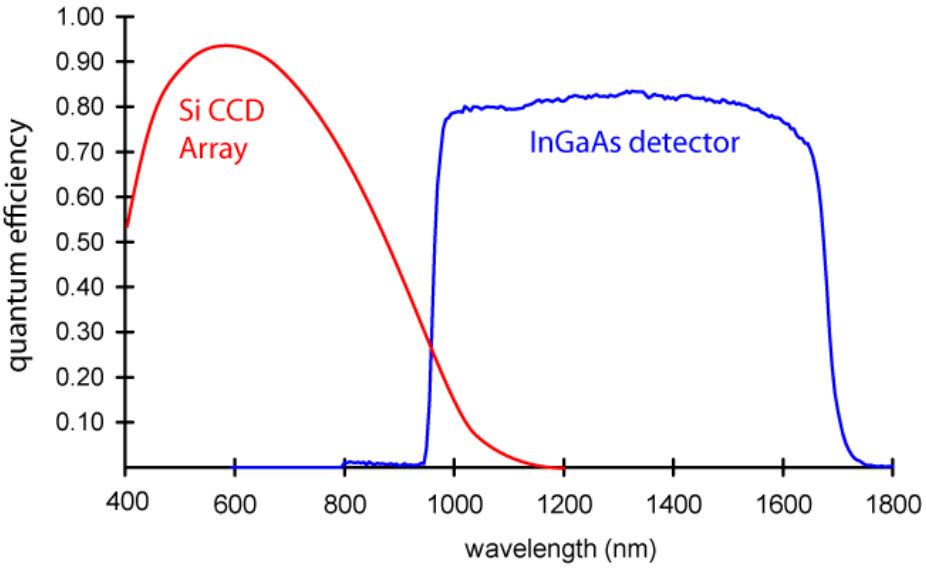

FIGURE 2-14: EFFICIENCY OF DIFFERENT DETECTOR AT CERTAIN WAVELENGTHS [6].

Since this detector is very costly, a commercially available silicon charged coupled device (CCD) camera was used to detect the light emitted at 1150 nm. The acquiring of the EL image should be done in a dark environment because the intensity of the near-IR light emitted by the PV module is relatively low compared to the radiation emitted by the environmental lighting. A high pass edge filter at 850 nm may be used to reduce interfering light from other sources because the Si CCD sensor is less sensitive to wavelengths of 1150nm [19, pp. 41–46].

To further reduce the influence of stray light, an image without current flowing through the PV cell will be taken and subtracted from the image with current flowing. With this method, cracks in the cell appear as dark lines, disconnects are visible by darker sections which have worse electrical properties whereas lighter sections have better electrical properties [19, pp. 41–46].

2.4.3 UV fluorescence

When EVA is exposed to sunlight, specifically the UV-spectrum, molecules in the encapsulation decompose to form lumophores. An UV-light (315 nm) can be used to excite the lumophores, which emit fluorescent light in the range of 325 – 800 nm. When oxygen comes in contact with the EVA, it will degrade the fluorescent lumophores to non-fluorescent lumophores. Oxygen is diffused through the back sheet to the EVA front layer of the module along the edges of and the cracks in the solar cells [19, pp. 47–48].

For UV-fluorescence (FL) imaging, an array of black light sources with a wavelength ranging from 310 nm to 400 nm may be used for the excitation. The source lamp typically has a light intensity at the module surface of 10-100 W/m². A longpass filter in front of the camera can be used to block the excitation light of the black light [19, pp. 47–48].

The PV module has to be exposed to sunlight for some time to develop lumophores. To get a sufficient fluorescence, the module should have been exposed to an UV dose of 80 kWh/m² (this equals 1,5 years outdoor exposure in Germany) [19, pp. 47–48].

On a FL-image, like Figure 2-15, it is possible to detect cell cracks. These cracks appear as dark bars on the cell. Due to the oxygen diffused through the back sheet, it is not possible to detect cracks at the cell edges [19, pp. 47–48].

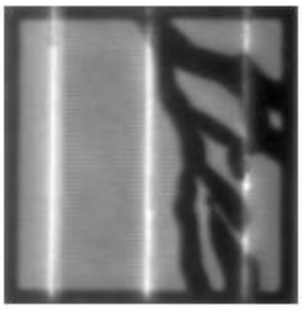

FIGURE 2-15: FL IMAGE OF CRACKS IN A CELL [19].

2.4.4 IV curve tracer

According to the standard measurements need to be done under illumination of light of 1 sun (1000 W/m²) with a light spectra of AM1.5G (reference spectrum of IEC 60904-3) at 25 °C. In order to keep the cell at 25 °C, it needs to be cooled. If this is not possible for the cell, a method where the lights flashes on the cell and the measurements are taken very quickly can be used An IV curve, as shown in Figure 2-16, is used to determine the Maximum Power Point (MPP) of a PV cell, module or system. Multiple measurements are needed to determine this point [6], [19, p. 26].

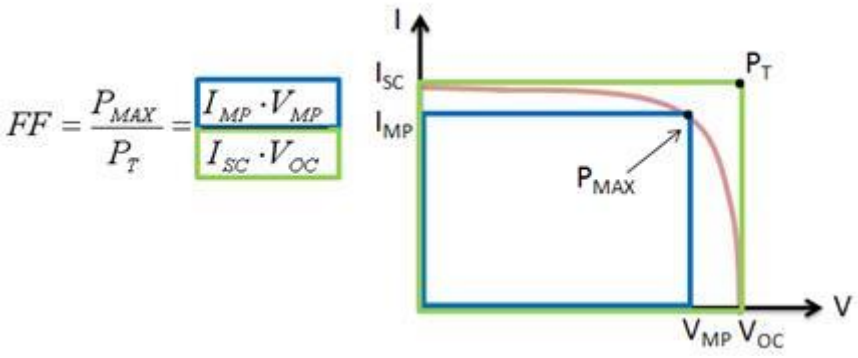

FIGURE 2-16: FILL FACTOR IN A IV CURVE [29].

The open-circuit voltage (Voc) is the maximum voltage available from a PV module when it is not supplying any current. The short-circuit current (Isc) is the current the module outputs when the voltage across the cell is zero volts. The maximum power (Pmax) is defined as the point on the IV curve of a PV module under illumination, where the multiplication of the current (I_{mp}) with the voltage (V_{mp}) is maximal. The Fill Factor (FF) is calculated by comparing the maximum power (P_{max}) to the theoretical power (P_T) and essentially is a measure of quality of the solar cell [6], [19, p. 26].

It is also possible to measure an IV curve in the dark. With this measurement the diode properties can be examined. There is a small difference between these methods because in the dark no light generated current will flow [30].

2.4.5 X-ray scanning

The X-ray scanning can be used to inspect alignment and delamination between the back sheet foil, the electrically conductive adhesive and the back contact cells. A 2D X-ray image of a single cell modules will make the locations where the copper was etched away from the back sheet, the electrically conductive adhesive visible on the close up image, the circular pattern of the silver metallization on the rear side of the cell, and the 8 straight metallization lines surrounding each laser drilled hole on the front side of the cell, as shown in Figure 2-17 [31, pp. 381–382].

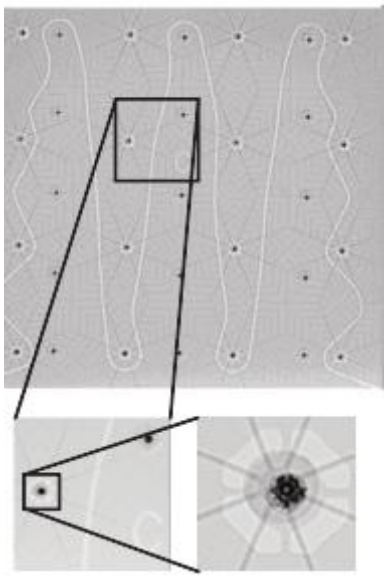

FIGURE 2-17: X-RAY SCANS OF BACK-CONTACT MODULES USING CONDUCTIVE FOIL [31, p. 382].

2.4.6 Ultrasonic scanning

Ultrasonic scanning uses sound waves as a non-destructive method to detect defects and can be used to detect air inclusions in PV modules, air inclusions will show up as black spot on the image, as shown in Figure 2-18. Ultrasonic scanning has a drawback in that water needs to be used as a medium between the transducer, receiver and the product under inspection. This will require a large water tank. In addition, this method is very time consuming as an image can take up to 30 minutes to be created [31, pp. 381–382], [32].

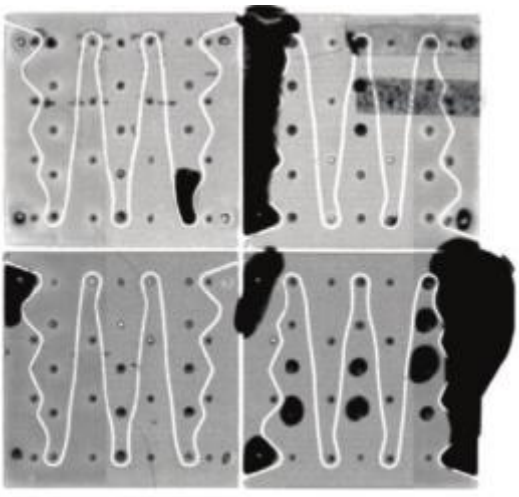

FIGURE 2-18: ULTRASONIC SCANS OF BACK-CONTACT MODULES USING CONDUCTIVE FOIL [31, p. 382].

Chapter 3 Materials and Methods

3.1 Hardware

3.1.1 High voltage source

A Keithley 6517A electrometer/high resistance meter, purchased from Keithley Instruments Inc. (Cleveland, OH, USA), was used during the PID-testing and is shown in Figure 3-1. The electrometer was used to supply the high voltage (1000 V) to the cell and can measure the currents as low as $10^{-12}\ A$. The built-in voltage source has a maximum power of one watt, this means that for different voltage ranges there are different maximum currents, as shown in Table 3-1 [33, p. 24].

TABLE 3-1: V-SOURCE RANGES OF THE KEITHLEY 6517A [33, p. 46].

Range	**Maximum output**		**Step size**
	Voltage	Current	
100 V	± 100 V	± 10 mA	5 mV
1000 V	± 1000 V	± 1 mA	50 mV

If the device reaches the maximum output current, it will automatically lower the voltage until it sources one watt of power. The device communicates through its GPIB interface. With a GPIB to USB interface it is possible to communicate with this device through LabVIEW [33, p. 24].

FIGURE 3-1: THE KEITHLEY 6517A ELECTROMETER/HIGH RESISTANCE METER USED FOR PID TESTS [34].

3.1.2 quadrant supply

The Keithley 228A voltage/current source, purchased from Keithley Instruments Inc. (Cleveland, OH, USA), was used to measure the IV curves of the PV modules. Figure 3-2 is the device that can sink and source a maximum of 100 W. The device can be used as a constant voltage or current source, the specification for each operating mode is showed Table 3-2 and Table 3-3 [35, p. 7].

TABLE 3-2: SPECIFICATIONS OF THE KEITHLEY 228A AS A CONSTANT VOLTAGE SOURCE [35, p. 7].

Range	Output			Compliance (Source or Sink)		
	Maximum (V)	Resolution	Accuracy (1 year) 18°-28°C	Maximum (A)	Resolution	Accuracy (1 year) 18°-28°C
100 V	± 101,0	100 mV	± (0,1 % + 0,1 V)	± 1,010	1 mA	± (0,1 % + 4 mA)
				± 0,1010	100 µA	± (0,1 % + 400 µA)
10 V	± 10,10	10 mV	± (0,1 % + 10 mV)	± 10,10	10 mA	± (0,5 % + 40 mA)
				± 1,010	1 mA	± (0,1 % + 4 mA)
				± 0,1010	100 µA	± (0,1 % + 400 µA)
1 V	± 1,010	1 mV	± (0,1 % + 1,0 V)	± 10,10	10 mA	± (0,5 % + 40 mA)
				± 1,010	1 mA	± (0,1 % + 4 mA)
				± 0,1010	100 µA	± (0,1 % + 400 µA)

TABLE 3-3: SPECIFICATIONS OF THE KEITHLEY 228A AS A CONSTANT CURRENT SOURCE [35, p. 7].

Range	Output (1 year 18°-28°C)			Compliance (Source or Sink)		
	Maximum (A)	Resolution	Accuracy (1 year) 18°-28°C	Maximum (V)	Resolution	Accuracy (1 year) 18°-28°C
10 A	± 10,10	10 mA	± (0,5 % + 10 mA)	± 10,10	10 mV	± (0,1 % + 40 mV)
				± 1,010	1 mV	± (0,1 % + 4 mV)
1 A	± 1,010	1 mA	± (0,1 % + 1 mA)	± 101,0	100 mV	± (0,1 % + 400 mV)
				± 10,10	10 mV	± (0,1 % + 40 mV)
				± 1,010	1 mV	± (0,1 % + 4 mV)
0,1 A	± 0,1010	100 µA	± (0,1 % + 0,1 mA)	± 101,0	100 mV	± (0,1 % + 400 mV)
				± 10,10	10 mV	± (0,1 % + 40 mV)
				± 1,010	1 mV	± (0,1 % + 4 mV)

FIGURE 3-2: THE KEITHLEY 228A VOLTAGE/CURRENT SOURCE USED FOR MEASURING IV CURVES OF PV MODULES [36].

3.1.3 Climate chamber

A Weiss SB22/160/80 climate chamber, as shown in Figure 3-3, purchased from Weiss Umwelttechnik (Reiskirchen-Lindenstruth, DE), was used to control the testing environment. Both the temperature and humidity can be controlled. The technical specifications are listed in Table 3-4.

TABLE 3-4: SPECIFICATIONS OF THE WEISS SB22/160/80 CLIMATE CHAMBER [37, p. 33].

Type number	**Temperature range**		**Humidity range**	**Temperature change gradient averaged according to DIN 50011, part 12**	
	Temperature control (°C)	Climate control (°C)	% RH	Cooling App. K/min	Heating App. K/min
160/80	-75 ... +180	+10 ... +95	10 ... 98	2,0	3,3

FIGURE 3-3: THE WEISS SB20 CLIMATE CHAMBER WITH A PV MODULE INSIDE READY TO MEASURE THE IV CURVE.

3.1.4 Solar simulator

A custom made solar simulator with an Atlas SolarConstant 1200 lamp, purchased from Atlas Material testing solutions (Mount Prospect, IL, USA), was used to simulate the sun for IV curve measurements.

The solar simulator has the following characteristics:

- daylight colour temperature of 5600 – 6000 K;
- flicker-free light, modulation < 1 %;
- capable of reaching an intensity of at least 1000 W/m².

3.1.5 Webcam

A Logitech C310,shown in Figure 3-4, purchased from Logitech (Lausanne, CH), was used for taking the EL images. The webcam has an effective number of pixels of 2560 x 1920 [38]. An EL image can be taken because the webcam is equipped with a Si CCD sensor [6]. To make the webcam useable for EL imaging, the IR-filter in front of the sensor has been replaced with a visible light filter. The visible light filter has been acquired by cutting a piece out of the end of a film roll.

FIGURE 3-4: THE LOGITECH C310 WEBCAM USED FOR TAKIN EL IMAGES

3.1.6 Reference PV cell

A Newport 91150V,show in Figure 3-5, purchased from Newport corporation (Irvine, CA, USA), was used to characterize the solar simulator. The reference cell has an operating temperature between 10 and 40 °C and it has a measuring range of 0 to 3,5 suns with a accuracy of 0,1 %. The reference cell comes with a meter that reads out the two by two cm calibrated solar cell and the thermocouple inside the reference cell assembly [39].

FIGURE 3-5: THE NEWPORT 91150V, ON THE LEFT IS THE METER AND ON THE RIGHT IS THE REFERENCE CELL ASSEMBLY [40].

3.1.7 Spectrometer

AvaSpec-3648-USB2-UA, show in Figure 3-6, purchased from Avantes (Apeldoorn, NL), is a fibre optic spectrometer. This was used to measure the spectral response of the solar simulator. The specifications are listed in Table 3-5.

TABLE 3-5: TECHNICAL DATA AVASPEC-3648 [41].

Features	AvaSpec-3648
Optical Bench	Symmetrical Czerny-Turner, 75mm focal length
Wavelength range	200 – 1100 nm
Resolution	0,025 – 20 nm, depending on configuration
Stray light	< 0,1 %
Sensitivity (AvaLight-HAL, 8µm fibre)	120000 counts/µW – per ms integration time
Detector	CCD linear array, 3648 pixels
Signal/Noise	300:1
AD converter	14 bit, 1 MHz
Integration time	10 µs – 10 minutes
Interface	USB 2.0 high speed, 480 Mbps or RS-232, 115.200 bps
Sample speed with on-board averaging	3,7 ms / scan
Data transfer speed	3,7 ms / scan
Digital IO	HD-26 connector, 2 Analog in, 2 Analog out, 3 Digital in, 12 Digital out, trigger, synchronization
Power supply	Default USB power, 440 mA. Or with SPU2 external 12 VDC, 440 mA
Dimensions, weight	175 x 110 x 44 mm (1 channel), 716 grams

It also has the options Slit-25 and OSC-UA. This means it has a usable range from 200 nm to 1100 nm.

FIGURE 3-6: THE AVASPEC-3648-USB2-UA USED FOR CHARACTERIZING THE SOLAR SIMULATOR [41].

3.2 Software

3.2.1 LabVIEW

LabVIEW is a system-design platform and development environment for a visual programming language, made by National Instruments. The programming language used is named “G”, which is a dataflow programming language. The execution of the code is determined by the structure of a graphical block diagram [42].

Programs and subroutines created by LabVIEW are called virtual instruments (VIs). Each VI consists out of 2 components: a front panel and a block diagram. The front panel is built using controls (inputs) and indicators (outputs). Through the controls a user can input values directly into the program. When a control or indicator is put on the front panel, they are automatically generated as nodes for use in the block diagram. The block diagram contains all the graphical source code. This also contains structures and functions. Which perform operations. These can be chosen from the functions palette. Controls and indicators from the front panel, as well as the functions and structures, are referred as nodes. The different nodes are connected by wires, which can be drawn. A node can only be executed as soon as all its input data has become available [42].

3.2.2 Autodesk Inventor

Autodesk Inventor is developed by the U.S. based software company Autodesk and is used to design, visualize and test product ideas. It is possible to create product prototypes that accurately simulate the weight, stress, friction, driving loads and more. The benefit of Inventor is that individuals familiar with using AutoCAD are put into a familiar design environment. Prototyping with Inventor can be easily accomplished by integrating 2D AutoCAD drawings and 3D data into a digital model which will serve as a virtual representation of the final product [43], [44].

Chapter 4 PID-test

The PID test are done following the IEC 62804-1 standard. This standard give 2 methods that can be used to stress a PV module against PID, the differences are listed in Table 4-1.

TABLE 4-1: DIFFERENCES BETWEEN THE METHODS FOR TESTING PID ACCORDING TO IEC 62804.

	Method a	**Method b**
Temperature of the module	60 °C ± 2 °C	25 °C ± 1 °C
Relative humidity	85 % ± 3 %	< 60 %
Dwell time	96 h	168 h
Leakage path	Grounded frame	Conductive foil
Necessary equipment	Climate chamber	/

4.1 Hardware

The setup to put -1000 V across the PV cell is shown in Figure 4-1. This is done because the tested PV cell was a p-type.

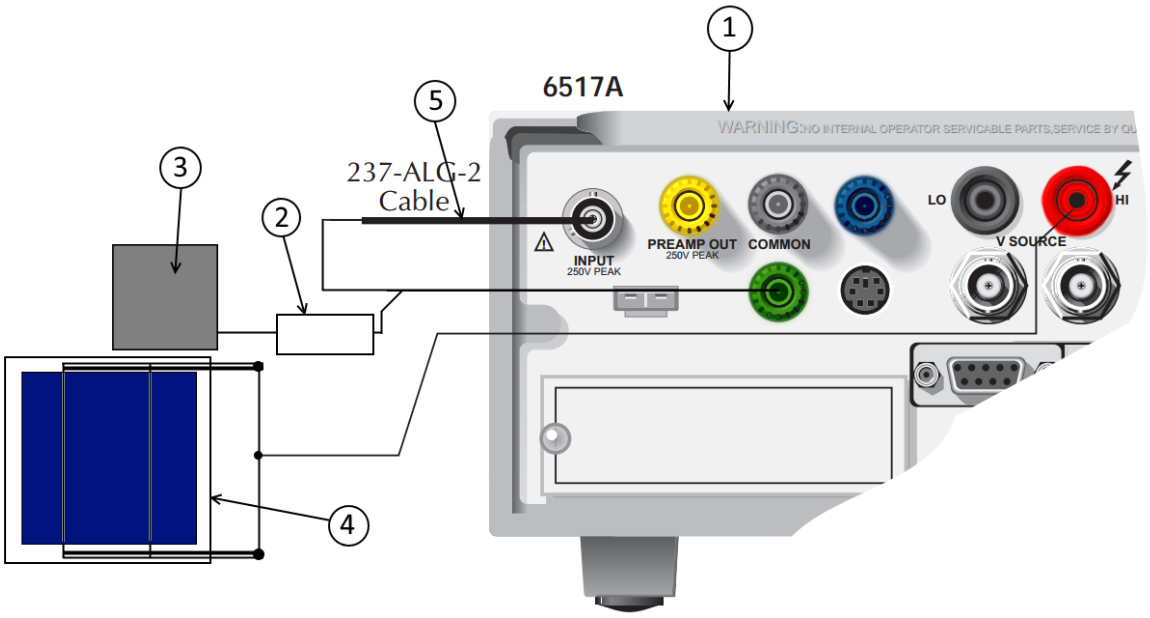

FIGURE 4-1: THE EXPERIMENTAL SETUP TO PUT -1000 V ACROSS THE PV CELL.

The -1000 V is provided by the Keithley 6517A (1). The connection of the PV module (4) will be short-circuited to make sure -1000 V is put across the PV module. The positive wire of the INPUT connector of the Keithley is connected to the ground and a resistor (2). The leakage current can be measured and logged because the INPUT is being used, this can be interesting to see if the forming migration Na-ions into the PV cell will increase the leakage current. A resistor of 1 kΩ and 10 W is connected to a conductive plate or foil (3). The resistor will limit the voltage that goes across the INPUT when a short circuit is formed between the PV module and the conductive plate or foil. An electron current will flow from the PV module to the conductive plate and thus creating a similar situation as PV modules in large strings. In case of curing, a voltage of 1000 V is put across the PV module. The PV module and the conductive plate are put into a climate chamber or an oven. Therefore the temperature and/or humidity of the chamber and thus also of the PV module can be controlled.

4.2 Software

To make all the devices easier to control and the initializing and logging of leakage current and IV curve tracing happen automatically, a program was created in LabVIEW. The user interface is shown in Figure 4-2.

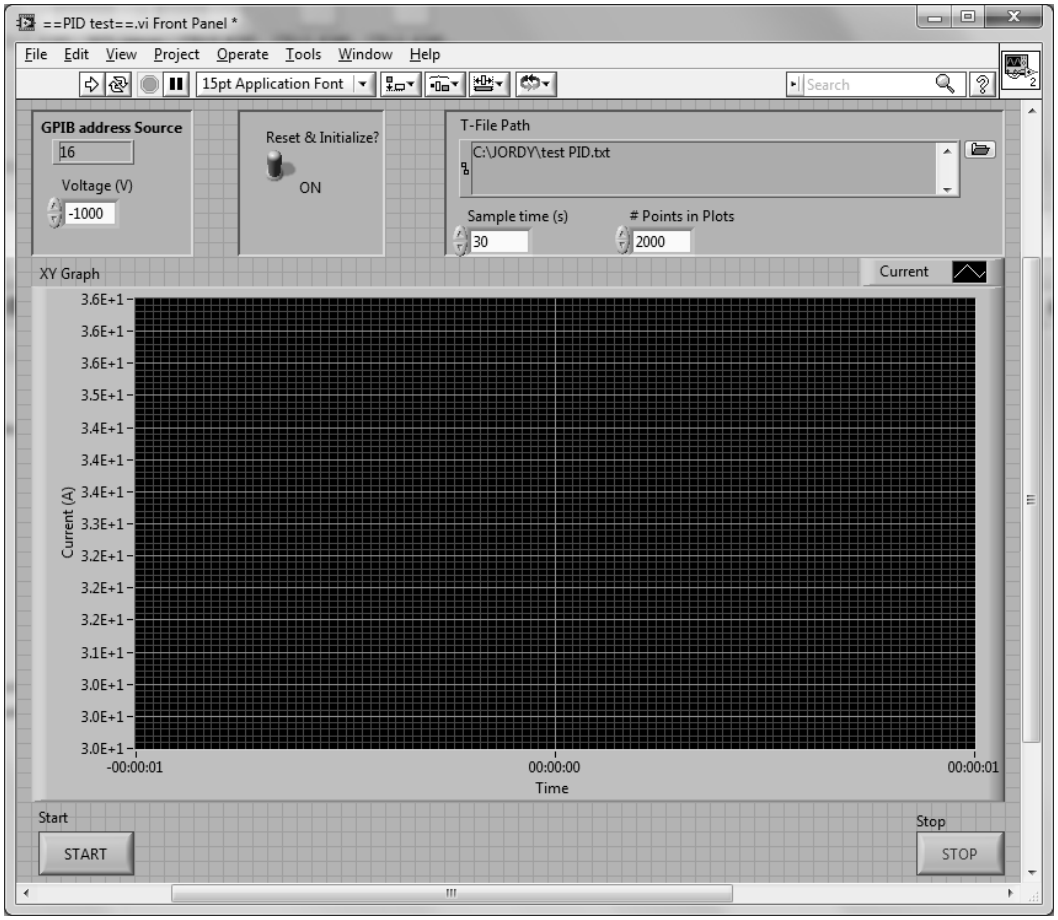

FIGURE 4-2: THE USER INTERFACE FOR CONTROLLING THE KEITHLEY 6517A FOR PID TESTING.

The voltage can be set that will be put across the PV cell and the conductive plate. Also a path can be chosen where the logging file will be saved.

4.3 Test results

Before PID testing, an IV curve and an EL image were taken in order to measure the initial parameters of the PV module. After the initial measurements, a PID test was performed by placing aluminium foil on top of the PV module and taping this down to ensure that the foil is in contact with the glass surface of the PV module. This setup was placed inside an oven in order to be able to regulate the temperature. The temperature inside the oven was regulated at 60 °C, which increases the severity of the PID test. Figure 4-3 shows the IV-curves of the initial measurement, after PID testing, and after PID curing.

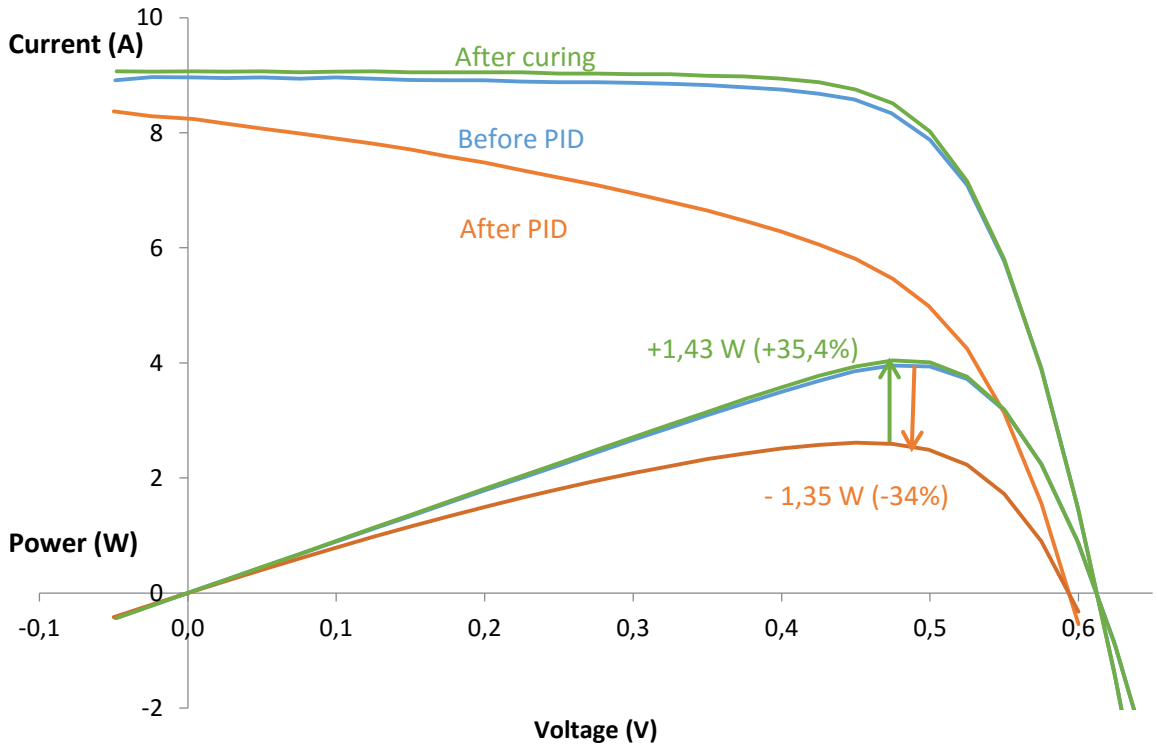

FIGURE 4-3: GRAPH SHOWING TEST RESULTS BEFORE AND AFTER PID, AND AFTER CURING.

The most notable difference between the initial measurement and measurement after PID testing is the shape of the IV curve; after PID testing, the curve is less horizontal at low voltages. This is an indication that the shunt resistance decreased, decreasing the efficiency of the module. After the curing process, the shape of the IV curve is recovered to its initial shape, indicating an increased shunt resistance and thus increasing the efficiency. This means that the degradation, caused by PID, has been reversed.

EL imaging is another way to detect PID because areas with a lower shunt resistance will show up as darker areas on the image. From the IV curves, it is clear that PID was present in the module. Therefore, a side by side comparison of the EL images before and after PID is shown in Figure 4-4.

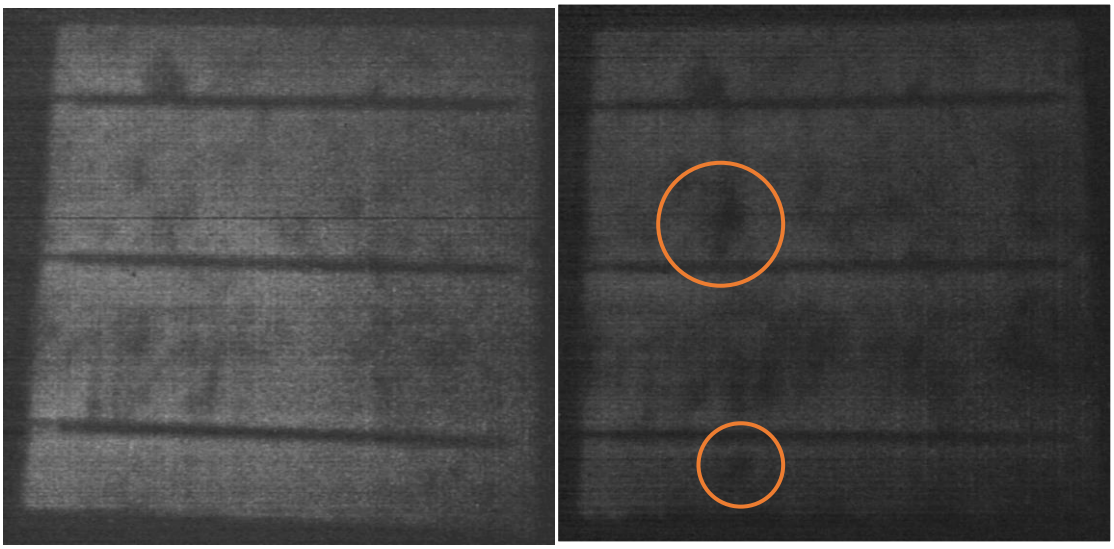

FIGURE 4-4: EL IMAGES OF THE SAME POLY CRYSTALLINE SILICON PV MODULE (LEFT) BEFORE PID AND (RIGHT) AFTER PID.

The PV module in the image at the right side is notably darker than the PV module in the image at the left side. This can be an indication of a lower shunt resistance of the entire PV module, but it can be possible that the webcam automatically changed the light intensity. However, a few even darker spots are visible. This can be an indication that on these locations Na-ions have migrated into the PV cell itself and that they are creating local shunts. However, no transmission electron microscopy method was used to prove this because of time constraints.

Figure 4-5 shows an EL image of the same PV module after the curing process. When this is compared to the EL image before PID testing, no remarkable differences could be noticed. This could indicate that the Na-ions were removed from the PV cell.

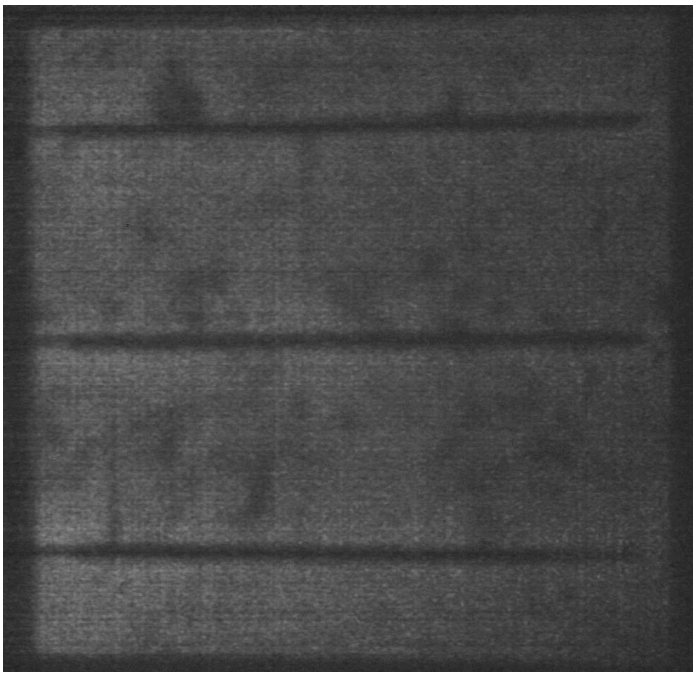

FIGURE 4-5: EL IMAGE OF THE SAME POLY CRYSTALLINE SILICON PV MODULE AFTER CURING.

Chapter 5 Setup designs

5.1 IV curve

5.1.1 Test setup

The four-quadrant source can measure the voltage locally or remotely. Local sensing is where the voltage is measured at the quick disconnect board. This means that the current and voltage is measured through the same cable, resulting in a voltage drop across the measuring cables. This creates a faulty measurement. Remote sensing uses different cables for measuring the current and the voltage. The different connection setups can be seen in Figure 5-1.

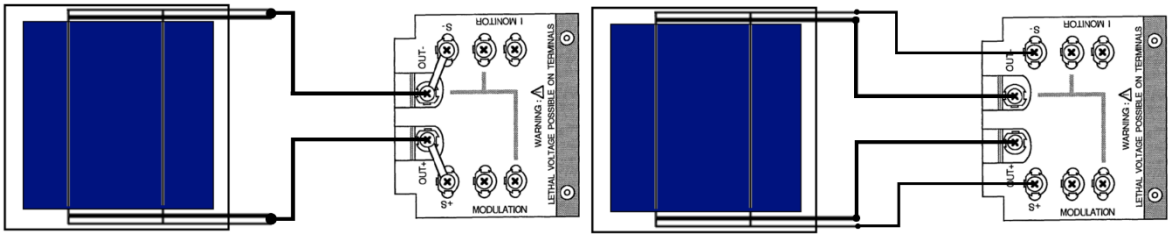

FIGURE 5-1: SETUP FOR LOCAL- (LEFT) AND REMOTE (RIGHT) SENSING FOR MEASURING IV CURVES.

What will follow is a manual describing the steps to measure an IV curve of a PV cell with a maximum I_{SC} of 10 A. Place the PV cell into the centre of the climate chamber and make sure the quick disconnect board is not plugged into the 4-quadrant source because, the output of the source is always connected even in standby modus. In standby modus it will try to keep the contacts at 0V. Connect the 4-wires to the PV cell for remote sensing, as is shown in Figure 5-1. Turn on the measuring device (4-quadrant source), input 0 A & 0 V and put the device in operating mode. If the amperage is negative and the voltage is positive it means that the PV cell is connected correctly. However, if the PV cell is not connected correctly, the quick disconnect board needs to be disconnected before making changes in the connection setup or else sparks will form on the contacts because a capacitor is placed between the OUT and SENSE connectors. After the connection has been made, open the VI called "==IV curve==" and Figure 5-2 will show up.

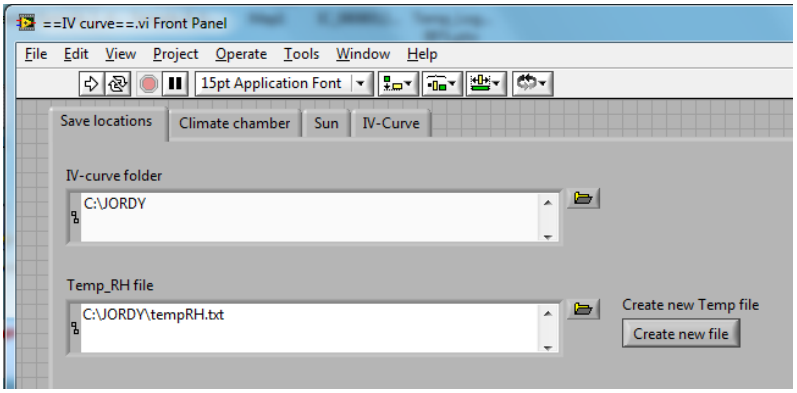

FIGURE 5-2: THE FIRST TAB OF THE USER-INTERFACE. FROM HERE YOU CAN CHOOSE THE LOCATIONS FOR THE LOG FILES.

The location chosen is where the files for the IV curves are automatically created. The other file location is where the temperature and humidity will be logged. If the file does not exist yet, the button "Create new file" can be pushed to automatically create the file. Close the climate chamber by putting the solar simulator in front of it. In the next tab, called "Climate chamber", the temperature and humidity of the climate chamber can be controlled, as seen in Figure 5-3.

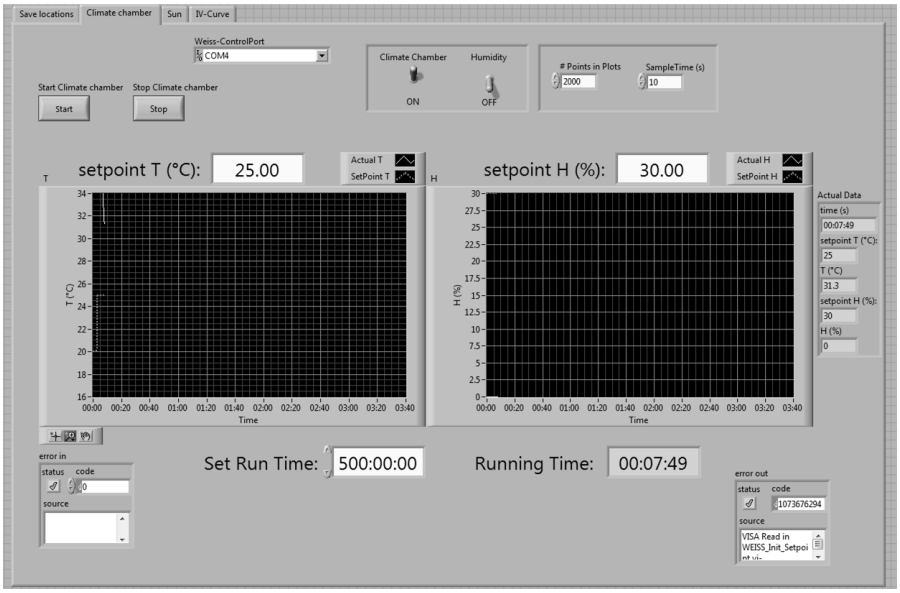

FIGURE 5-3: THE CLIMATE CHAMBER TAB OF THE USER INTERFACE. FROM HERE THE CLIMATE CHAMBER CAN BE STARTED AND THE SET POINTS CAN BE CHOSEN.

In this tab the climate chamber can be turned on and off. By changing “Humidity”, the humidity can be controlled by changing the value for “set point H(%)”. The tab “Sun” can only be used to turn the solar simulator on and off. The intensity needs to be changed manually at the ballast of the solar simulator. Controlling the intensity from the pc is unreliable because it is impossible to read the current intensity value from the ballast. The tab “IV curve” , shown in Figure 5-4, is where an IV curve of the PV cell can be measured.

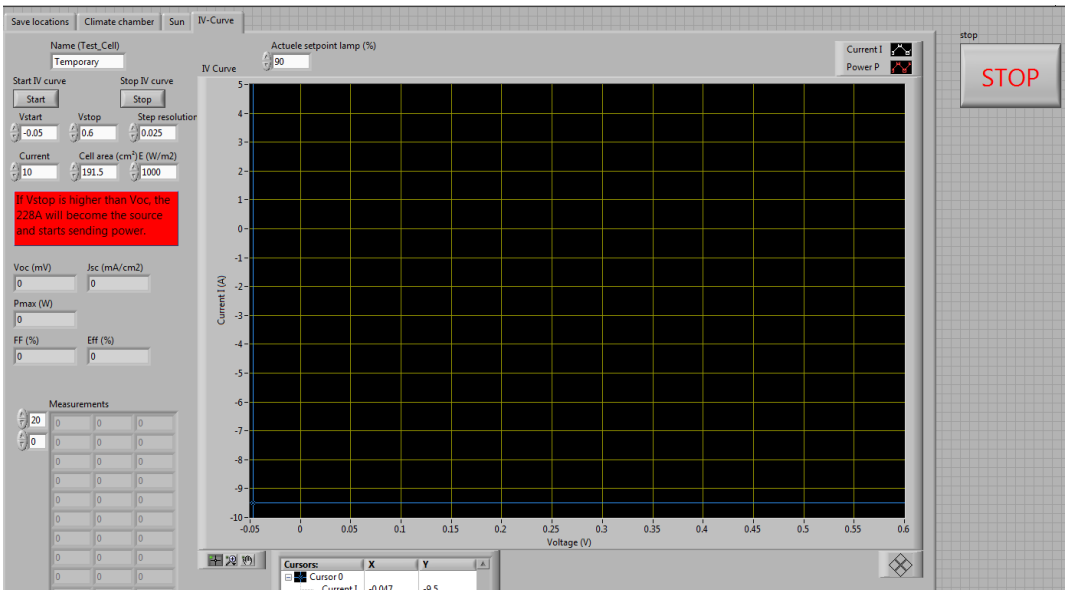

FIGURE 5-4: THE TAB OF THE USER INTERFACE FOR MEASURING THE IV CURVE.

It is required to put the name of the PV cell into “Name (test_cell)”, this name is used to name the files of the IV curves, as is the value for the “Actual set point solar simulator (%)”. To start measuring an IV curve, the button “Start IV curve” has to be pressed. The shutter opens before a measurement and closes after a measurement automatically. When all the measurements are done, pressing the big, red “Stop” button, located to the right side of the VI, turns everything off. Before disconnecting the PV cell make sure the quick disconnect board of the 4-quadrant source is disconnected.

The conclusion is that the measurement of the IV curve is easy and happens automatically. A thing that can be improved is to measure the temperature of the cell. This makes it possible to correct the IV curve . Another solution is to purchase a faster measuring device, so that the PV cell has less time to heat up by the irradiance of the solar simulator. A reference cell should be used periodically to check if the solar simulator is outputting the power that equals 1 sun (1000 W/m²), because the lamp in the solar simulator will degrade over time.

5.2 Shutter

5.2.1 Introduction

According to the IEC 60904-3 standard, the PV cell has to be at a temperature of 25 °C ± 2 °C. This is not possible with the current solar simulator setup because it needs to heat up in order to emit 1 sun and be as close as possible to the AM1.5 spectrum. During the time the solar simulator heats up, the PV cell will heat up because of the light emitted by the solar simulator. Therefore a modification to the setup was needed, so that the solar simulator can heat up and the emitted light would not be able reach the PV cell.

The shutter on the solar simulator was already driven by servomotors. The problem was that the servomotors lost their position after a few cycles, causing them tohit the walls of the solar simulator and not closing properly.

5.2.2 Setup

It was chosen to use pneumatic swivel actuators because of the problem with the loss of position. A swivel module from Festo was chosen and the semi-rotary actuators, swivel module DSM, were chosen because of the option to adjust the swivel angle. The largest concern was the moment of inertia of the shutter doors. The actuators need to be able to handle these forces without damaging itself. The shutter doors are rectangles made from aluminium and the dimensions are shown in Table 5-1.

TABLE 5-1: THE DIMENSIONS OF THE SHUTTER DOORS.

	Door 1	**Door 2**
Height (mm)	620	620
Width (mm)	160	180
Thickness (mm)	2	2

The largest door was then drawn in Inventor with the material chosen as aluminium 6061. Inventor then calculated the moment of inertia and the result was $244{,}99 * 10^{-4}\ kgm^2$. A swivel actuator was then chosen that could withstand the inertia and is able to open the shutter doors in less than a second . The graphs in the documentation for the swivel modules DSM were consulted and the DSM-25-270-P1 was chosen because of the faster swivel time for a 90 ° angle, as shown in Figure 5-6.

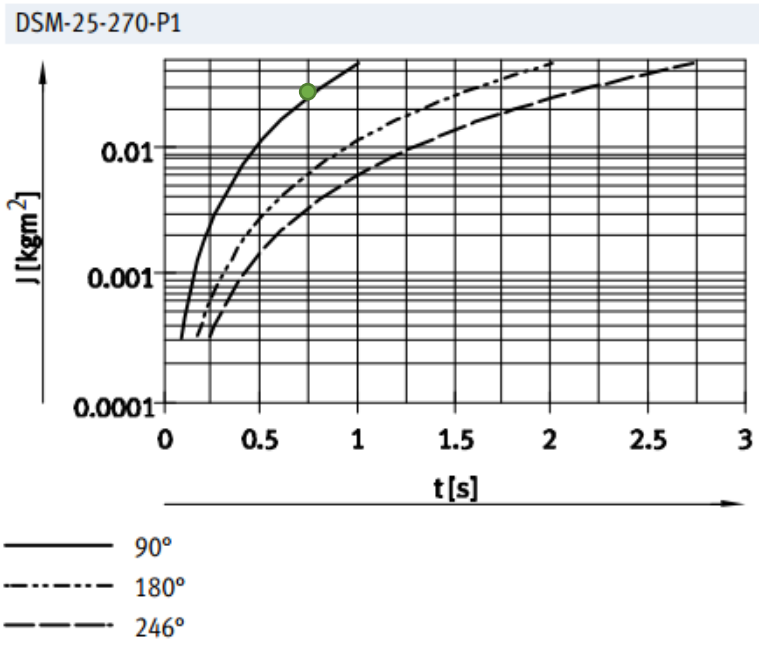

FIGURE 5-5: MASS MOMENT OF INERTIA J AS A FUNCTION OF SWIVEL TIME T WITH ADJUSTABLE, ELASTIC CUSHIONING COMPONENTS (P1) [45, p. 34].

From this graph, it can be concluded, that the maximal inertia is $500 * 10^{-4}\ kgm^2$ and that it would take about 0,75 s to achieve a 90° rotation, which is sufficient for our setup.

A mono-stable 2/5 valve controls the pneumatic, actuators; therefore the swivel actuators will be closed in case of a power outage or another problem. This is preferred so that the sample in the climate chamber will not be degraded by the intensity of the light and the heat resulting from the intense light.

An Arduino was chosen to control the pneumatic valves because the Arduino can be controlled from within LabVIEW. The Arduino runs on 5 V while the pneumatic valves need 24 V. Therefore, an electronic circuit has been made to allow the Arduino to control the pneumatic valves. This was achieved by using MOSFETs, that can be controlled by an Arduino using a 5 V signal, controlling the 24 V required for the pneumatic valves. The complete electronic circuit is shown in Figure 5-6.

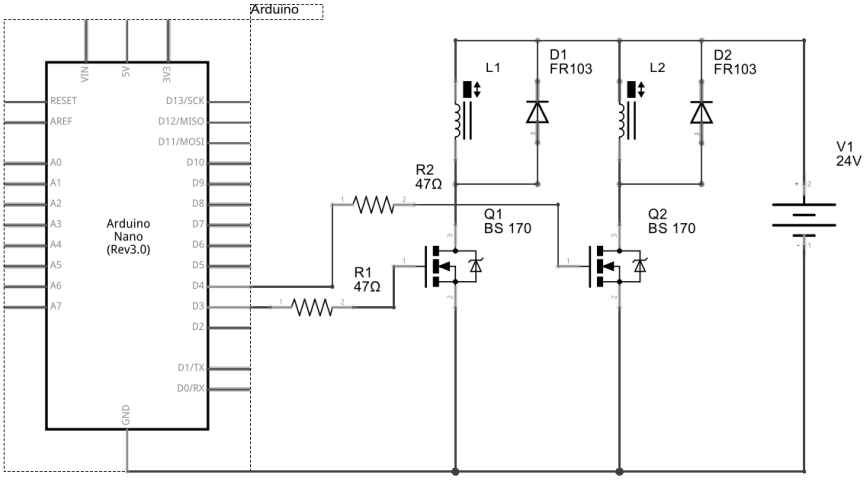

FIGURE 5-6: ELECTRICAL DIAGRAM FOR CONTROLLING THE PNEUMATIC VALVES WITH THE ARDUINO.

The implementation of the shutter into the VI for measuring IV curves is simple. Therefore the shutters will be automatically controlled when measuring IV curves. The shutter has been used for over 60 times without any problem. Since the shutter is frequently being used, it can be concluded that the setup of the shutter is reliable.

5.3 EL imaging

5.3.1 Setup

The setup created for acquiring an EL image of a PV cell is shown in Figure 5-7.

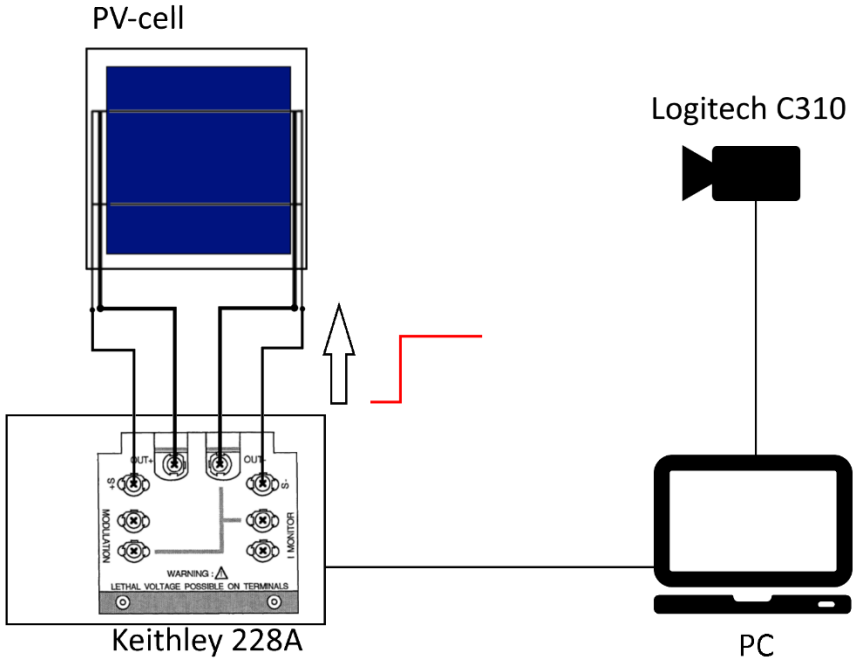

FIGURE 5-7: THE SETUP FOR TAKING EL IMAGES OF A PV CELL.

The Keithley 228A supplies the I_{sc} to the PV cell, which is a direct current. The PC will communicate with the Keithley 228A and the Logitech C310 webcam in order to make the process automated. The LabVIEW software does the imaging processing because this is necessary to create an image with a higher contrast and less noise. The difference the LabVIEW software does can be seen in Figure 5-8.

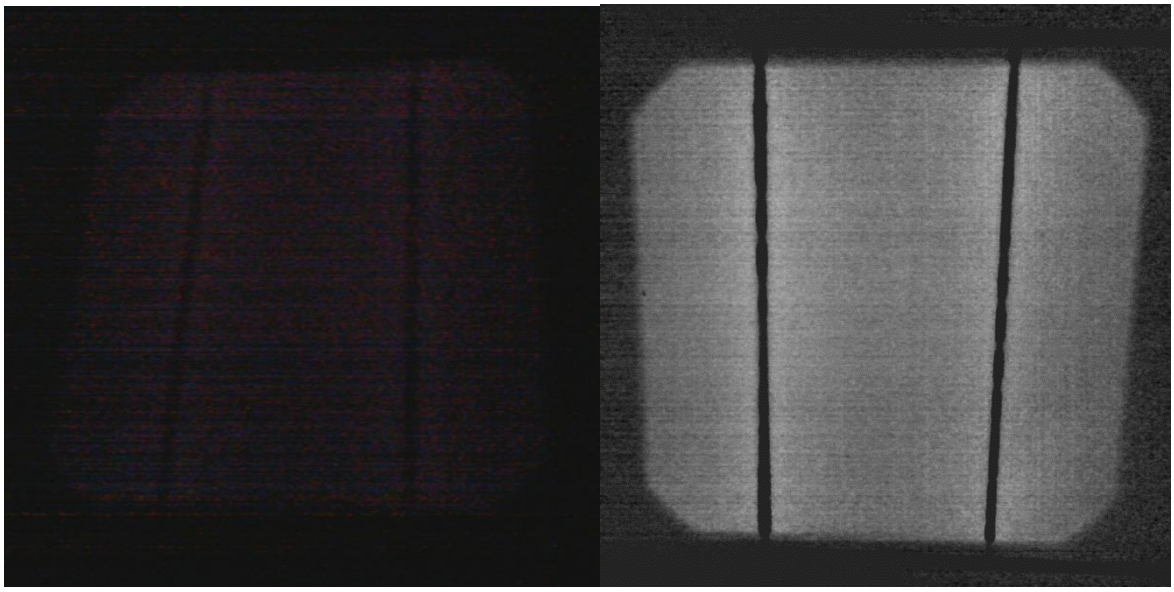

FIGURE 5-8: EL IMAGES OF THE SAME PV CELL WHEN A CURRENT OF 7A IS APPLIED. ON THE LEFT SIDE IS A SINGLE IMAGE TAKEN BY THE WEBCAM AND ON THE RIGHT IS AN IMAGE AFTER IT WENT THROUGH THE IMAGE PROCESSING.

This is achieved by following these steps:

- By turning the colour image into a grayscale image;
- Average a number of pictures without applying a current through the single cell PV module;
- Average a number of pictures while applying a current through the single cell PV module;
- Subtract both resulting images from each other.

It is possible to take these EL images while the light in the room is turned on. It is necessary that a reflection of a lamp is not visible in the PV cell; this will cause an oversaturated spot in the EL image.

Chapter 6 Characterization of the solar simulator

6.1 Introduction

IV measurements of PV modules are conducted indoors with a solar simulator. The advantage of an indoor measurement is that the measurement is not dependent on the weather conditions. However solar simulators are not light sources that can replicate the sun and the quality of the emitted light can strongly influence the results of the IV measurement. The parameters that must be considered are: uniformity of irradiated intensity in the test area, spectral irradiance distribution of the lamp and the temporal instability of the irradiated intensity [46, p. 23].

6.2 Standard

6.2.1 Temporal stability of emitted light

The irradiance is not completely stable but it will fluctuate. This means that during an IV sweep the generated photocurrent will follow these fluctuations, which can lead to measurement errors [46, p. 24].

6.2.2 Non-uniformity of irradiance

When individual cells in a PV module are not uniformly illuminated, the cells will deliver different currents. Therefore these cells will operate at a negative voltage range and they will have a negative contribution to the module voltage, which leads to a deformation of the IV curve in comparison to the ideal case for uniform irradiation, as show in Figure 6-1 [46, p. 24].

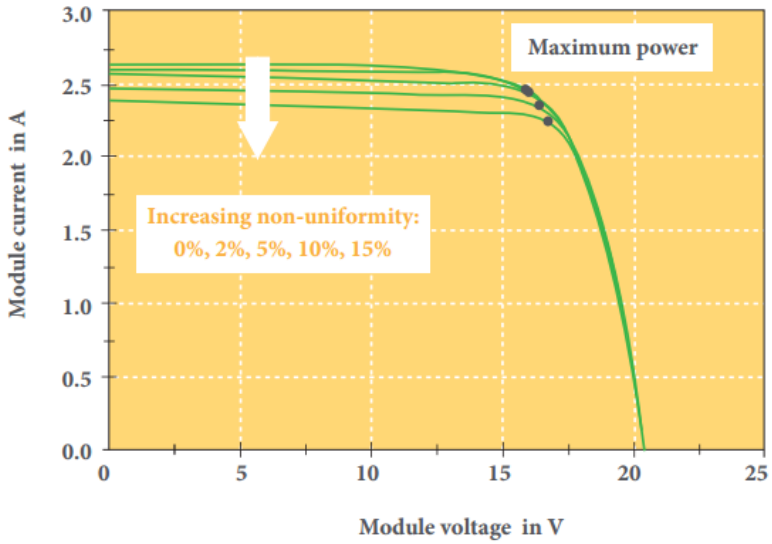

FIGURE 6-1: EFFECT OF NON-UNIFORMITY OF THE SOLAR SIMULATOR ON IV MEASUREMENTS [46, p. 24].

6.2.3 Spectral mismatch to AM1.5 reference spectral irradiance

The response of solar cells is strongly dependent on the wavelength. Xenon light sources are normally used for solar simulator. However, the spectral irradiance of a Xenon lamp differs slightly from AM1.5 spectral irradiance. This spectral irradiance mismatch may lead to a measurement error [46, p. 23].

6.2.4 Classification

The standard IEC 60904-9 defines a method to classify a solar simulator. Table 6-1 shows three quality indicators and the classification.

TABLE 6-1: CLASSIFICATION OF SOLAR SIMULATORS FOR POWER MEASUREMENT [46, p. 25].

Quality indicator	**Method**	**Classification**		
		A	B	C
Non-uniformity of irradiance	Monitoring of irradiance distribution in the test area. Calculation from measured Min/Max values of irradiance.	< 2 %	< 5 %	< 10 %
Spectral match to AM 1.5 reference spectral irradiance (IEC 60904-3)	Ratio of irradiance contributions of 6 wavelength ranges (400-500-600-700-800-900-1100): Solar simulator/AM 1.5 reference	0,75 to 1,25	0,6 to 1,4	0,4 to 2,0
Temporal stability of emitted light (LTI = Long Term Instability)	Monitoring of irradiance at a fixed position in the test area. Calculation from Min/Max values during IV data acquisition time	< 0,5 %	< 2 %	< 10 %

6.3 Test method

First the centre of the climate chamber had to be determined, so the inside of the chamber got measured. The dimensions are 555 mm x 435 mm x 670 mm (W x D x H). This means that the centre is located at 277,5 mm x 217,5 mm x 335 mm. Secondly the reference PV cell was placed at the centre of the chamber. As last the distance of the solar simulator was adjusted until the reference cell gave a measurement of 1 sun (1000 w/m²).

6.3.1 Temporal stability of emitted light

The temporal stability was measured with the reference PV cell during 130 minutes. Afterwards, a timeframe of 50 minutes was chosen where the temperature of the reference cell was most consistent, as show in Figure 6-2.

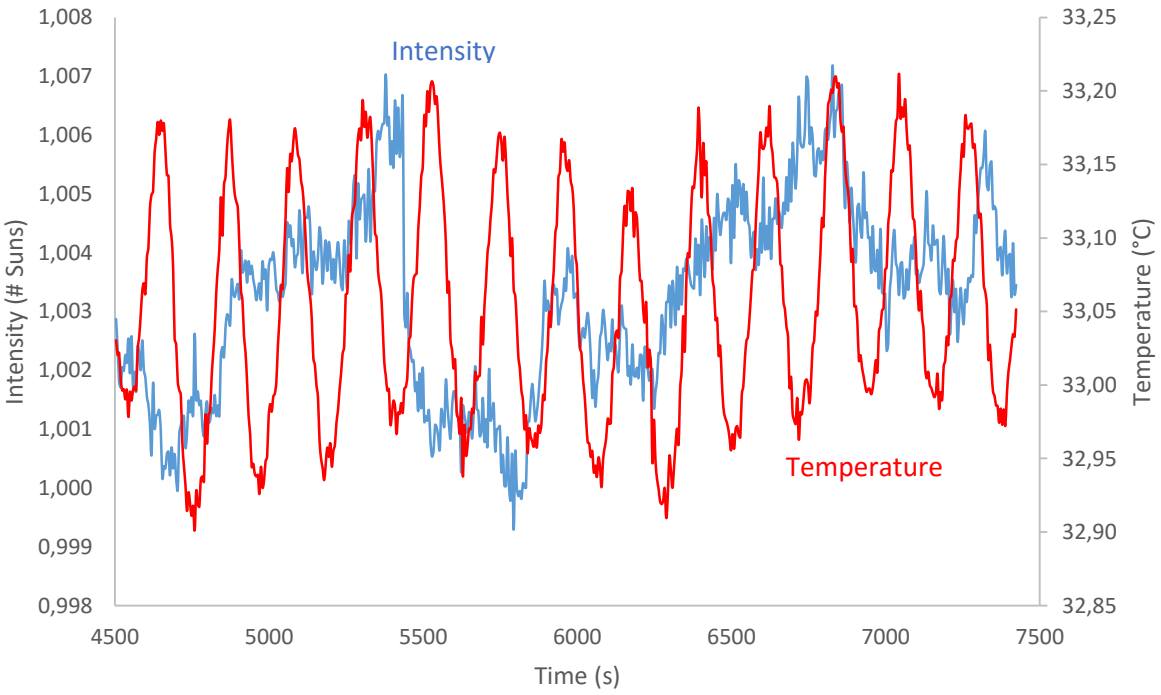

FIGURE 6-2: TEMPORAL STABILITY MEASUREMENT OF THE REFERENCE CELL.

6.3.2 Non-uniformity of irradiance

The non-uniformity was measured after the stability test. This means that the solar simulator is warmed up and outputting an intensity of 1 sun in the centre. The reference PV cell used has the following dimensions; 20 mm x 20 mm. Because of the small size of the reference PV cell, it was too time consuming to measure the entire area. Therefore, it was chosen to move the reference cell with a distance of 100 mm in between measurements, until the cell hit the side walls of the climate chamber, as shown in Figure 6-3.

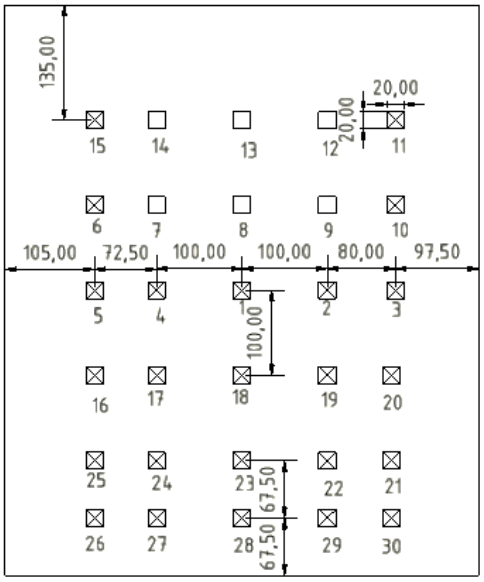

FIGURE 6-3 POSITION OF THE REFERENCE PV CELL FOR EACH MEASUREMENT.

6.3.3 Spectral match to AM1.5 reference spectral irradiance

The spectrum was measured using the fibre optic spectrometer with a range from 200 – 1100 nm. This was done after the solar simulator had warmed up for 15 minutes and the result is seen in **Fout! Verwijzingsbron niet gevonden.**

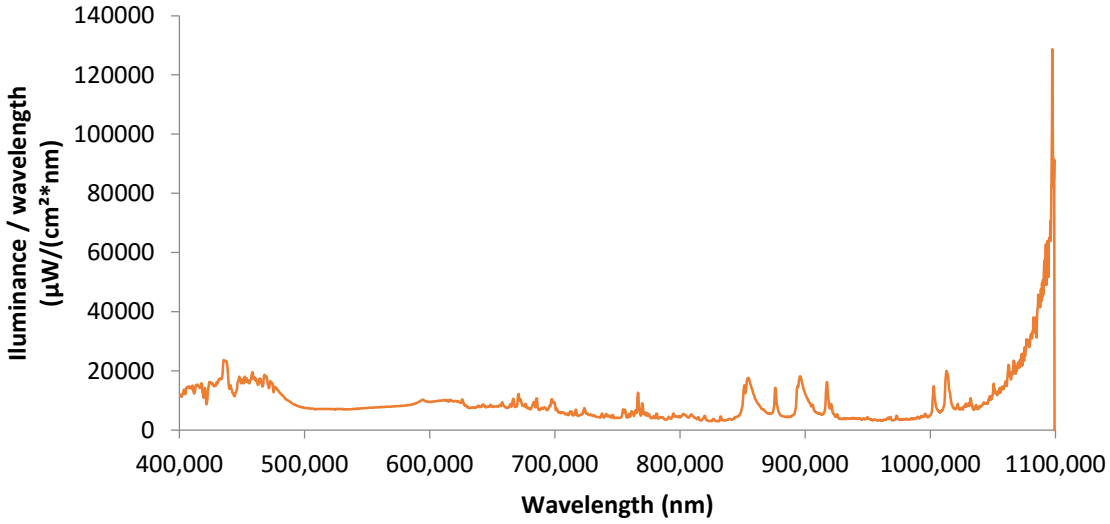

FIGURE 6-4: THE MEASURED SPECTRAL RESPONSE OF THE SOLAR SIMULATOR.

The allowed deviation from the ideal values is showed in Table 6-1. The ideal values were taking from [47].

6.4 Results

6.4.1 Temporal stability of emitted light

According to [46, p. 25] the deviation is calculated from the measured Min/Max values during the data acquisition time for an IV curve. Equation 6-1 shows how the deviation is calculated.

$$\boldsymbol{Dev = \left(1 - \frac{Min}{Max}\right) * 100} \qquad (6\text{-}1)$$

From Figure 6-2 we get the maximum value for the intensity (1,007) and the minimum value (0,999). If we put these values in the equation, we get a deviation of 0,7%. This indicated that for temporal stability we have a class B solar simulator.

6.4.2 Non-uniformity of irradiance

The measured values and positions are then put into a custom made LabVIEW program. These values have been plotted into a 3D plot, where the intensity is the Z axis. The measured points are plotted in a 2D-graph and is shown in Figure 6-5.

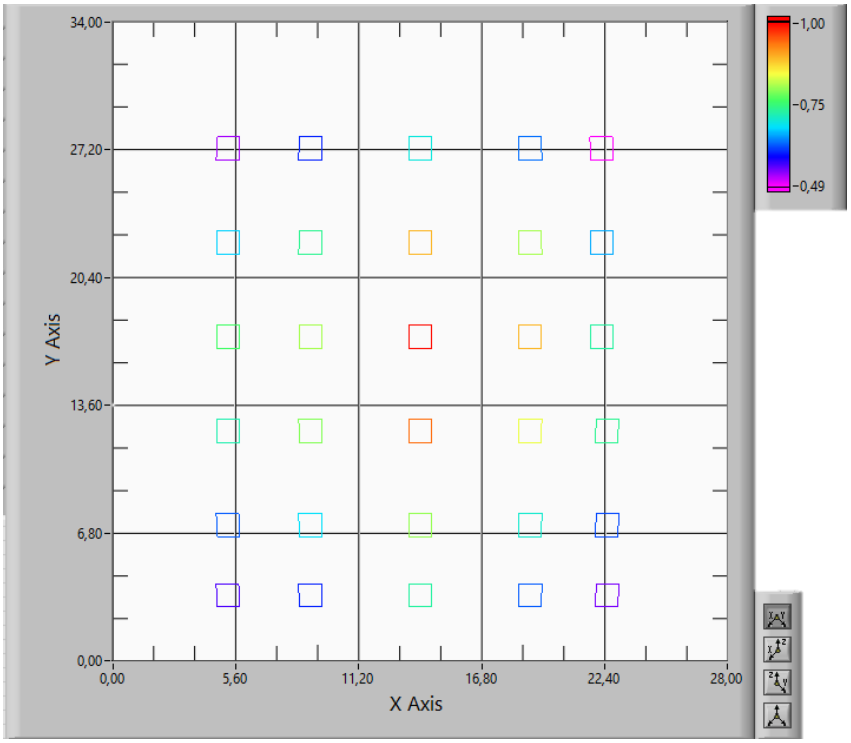

FIGURE 6-5: VALUES AND POSITIONS OF THE MEASUREMENTS.

This information is not enough to determine the uniformity of the solar simulator. Therefore, the values are interpolated with the bi-harmonic spline method and also plotted into a 3D plot. The resulting X-Y plane is shown in Figure 6-6.

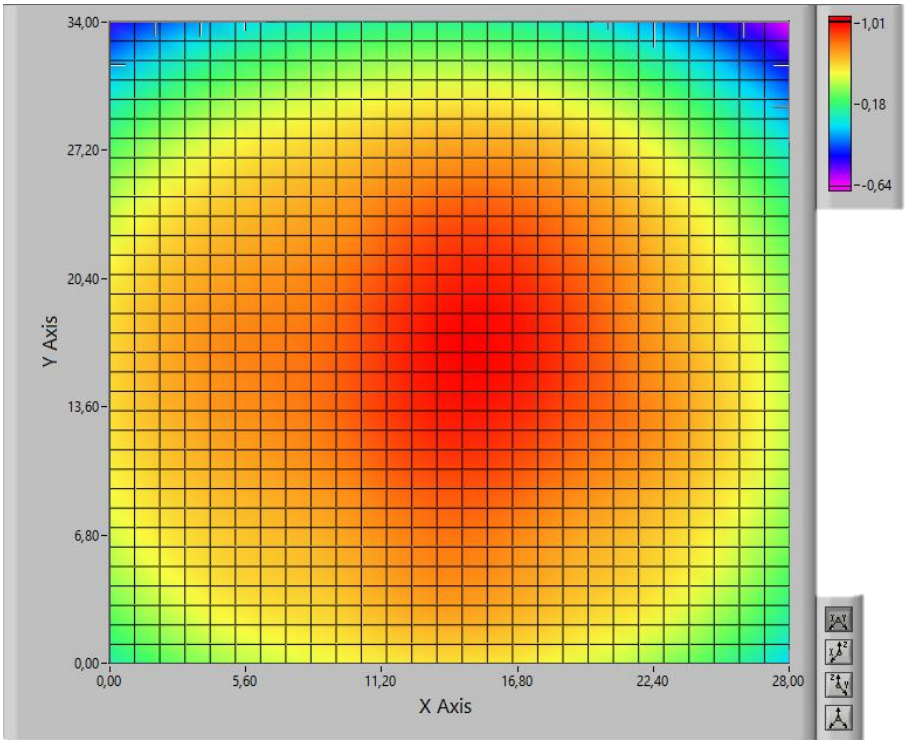

FIGURE 6-6: INTERPOLATED VALUE AND POSITION OF THE INTENSITY.

With this information we can give a more accurate assumption of the uniformity. We can see that the uniformity is elliptical. To determine the size and position of the ellipses for the different classes, the X-Z and Y-Z plots are used. These can be seen in Figure 6-7.

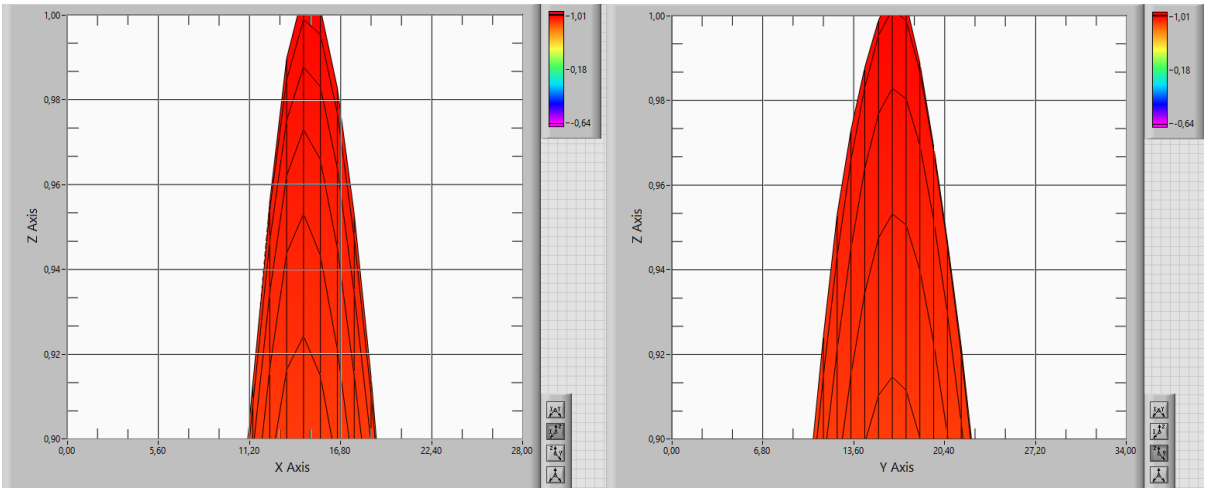

FIGURE 6-7: THE FIGURES SHOW THE AREA IN WHICH THE DEVIATION IS <10%. THE LEFT FIGURE IS THE X-Z PLANE AND THE RIGHT IS THE Y-Z PLANE.

Out of these plots the size and position of the ellipses for the classes A, B and C can be determined. The calculated sizes and positions can be seen in Table 6-2 for every class.

TABLE 6-2: SIZE OF THE ELLIPSE AND DISTANCE TO THE CENTRE OF THE ELLIPSE FOR EACH CLASS.

Class	**Minor Axis as width (cm)**	**Major Axis as height (cm)**	**Distance to centre from the bottom left corner of the climate chamber**	
			Width (cm)	Height (cm)
A (< 2 %)	6,91	10,43	30,15	33,32
B (< 5 %)	10,83	16,32	30,05	33,10
C (< 10 %)	16,05	24,02	30,24	33,32

6.4.3 Spectral mismatch to AM1.5 reference spectral irradiance

The values of the measured spectrum are averaged within their wavelength range. Thereafter, the relative averages from the sum of all the averages are calculated and these are show in Table 6-3.

TABLE 6-3: THE VALUES FOR THE IDEAL RELATIVE VALUES, UPPER LIMIT (UL) AND LOWER LIMIT (LL) ARE PUT INTO THE RIGHT PART OF THE TABLE. THE LEFT PART OF THE TABLE SHOWS THE MEASURED VALUES AND THE CLASS THEY BELONG TO.

Wave length range (nm)	**Ideal (%) IEC**	**Class A**		**Class B**		**Class C**		**Calculated**	
		UL (*1,25)	LL (*0,75)	UL (*1,4)	LL (*0,6)	UL (*2)	LL (*0,4)	Value (%)	Class
400-500	18,5	23,1	13,9	25,9	11,1	37	7,4	24,7	B
500-600	20,1	25,1	15,0	28,1	12,1	40,2	8,0	14,0	B
600-700	18,3	22,9	13,7	25,6	11,0	36,6	7,3	15,5	A
700-800	14,8	18,5	11,1	20,7	8,9	29,6	5,9	9,9	B
800-900	12,2	15,3	9,2	17,1	7,3	24,4	4,9	12,6	A
900-1100	16,1	20,1	12,1	22,5	9,7	32,2	6,4	23,3	C

From Table 6-3 we can determine that the solar simulator is rated a class C for spectral mismatch.

Chapter 7 Conclusion

PID is a degradation that can cause a big drop in efficiency of a PV module. Efficiency measurements and EL imaging are valid measuring technique to conclude if PID is present in a PV module. Efficiency measurements have the advantage of being able to quantify the amount of PID, but this setup needs big and expensive equipment, like a solar simulator, a climate chamber to keep the temperature of the PV module stable and a device that can apply different loads to the PV cell. EL imaging is a fast and simple measuring technique. The cost of the camera depends on the desired sensitivity and resolution of the camera. The only equipment needed is a power source capable of sourcing the Isc of the PV module and an EL camera, as discussed in 0 and 2.4.4.

During the course of this master's thesis, a demo setup for PID testing, IV curve measurements and EL imaging were created. The hardware and software used are explained in Chapter 3. The setup was tested with a single cell, poly-crystalline PV module in order to create comparable results. Therefore, it was easier to conclude the effective functioning of the setup.

After submitting the PV module to the PID test and measurement methods, it can be concluded that the PID setup can accelerate and cure PID in a PV module. The amount of PID was quantified by the change in efficiency of the PV module. After a PID test of 1 week, a decrease of 34 % of the initial power was achieved, the curing process increased the efficiency of the PV cell again by 35,4 %. On the EL images it was not clearly visible if the PV module was degraded by PID. This can be further improved by acquiring a cooled EL camera with a InGaAs sensor and a higher sensitivity for light with a wavelength of 1150 nm. A high resolution is required in order to be able to pinpoint the exact location where PID subsided.

A shutter has been developed to make sure the PV module does not heat up during the heat up process of the solar simulator. Therefore, more accurate measurements can be done and the measurements can be compared to measurements found in publications.

During this master's thesis, a setup was designed for measuring an IV curve while a PV cell is positioned vertically. This setup has not been realised because of the decision to test PID on laminated PV modules instead of not laminating the modules. The reason for not laminating the modules is because then it is possible test different materials against PID.

At the end of this master's thesis, it can be concluded that the demo setup for PID testing, is working. For PID testing, it can be interesting to use wires that are insulated for 1000 V in order to make sure the measured leakage current is current leaking through the PV module and not current leaking through the climate- or oven chamber. IV curve measurements are done using a4 quadrant power source, a Keithley 228A. This device needs an average of one second for each measurement point. Therefore, it was chosen to measure fewer point for the IV curves then the temperature of the PV module would stay within the standard test conditions. This can be solved by acquiring a faster IV curve sweeping device.

Chapter 8 References

[1] V. Naumann, D. Lausch, A. Graff, M. Werner, S. Swatek, J. Bauer, A. Hähnel, O. Breitenstein, S. Großer, J. Bagdahn, and C. Hagendorf, "The role of stacking faults for the formation of shunts during potential-induced degradation of crystalline Si solar cells," *Phys. status solidi - Rapid Res. Lett.*, vol. 7, no. 5, pp. 315–318, May 2013.

[2] Advanced Energy, "Understanding Potential Induced Degradation," 2012.

[3] K. Mishina, A. Ogishi, K. Ueno, T. Doi, K. Hara, N. Ikeno, D. Imai, T. Saruwatari, M. Shinohara, T. Yamazaki, A. Ogura, Y. Ohshita, and A. Masuda, "Investigation on antireflection coating for high resistance to potential-induced degradation," *Jpn. J. Appl. Phys.*, vol. 53, no. 3S1, p. 03CE01, Jan. 2014.

[4] M. B. Koentopp, C. Taubitz, M. Schütze, Kröber, and Marcel, "A PID model ensuring 25 years of service life nrel," 2015. [Online]. Available: http://www.nrel.gov/pv/performance_reliability/pdfs/2015_pvmrw_114_koentopp.pdf. [Accessed: 31-Aug-2015].

[5] P. Hacke, R. Smith, K. Terwilliger, G. Perrin, B. Sekulic, and S. Kurtz, "Development of an IEC test for crystalline silicon modules to qualify their resistance to system voltage stress," *Prog. Photovoltaics Res. Appl.*, vol. 22, no. 7, pp. 775–783, Jul. 2014.

[6] C. Honsberg and S. Bowden, "PV Education." [Online]. Available: http://www.pveducation.org/. [Accessed: 17-Aug-2015].

[7] A. S.H., "The doping of Semiconductors." [Online]. Available: http://ummalqura-phy.com/HYPER1/dope.html. [Accessed: 05-May-2016].

[8] M. H. Weik, *Fiber Optics Standard Dictionary*, Third Edit. Boston, MA: Springer US, 1997.

[9] Mega solar Systems, "How the Solar Power System Works?" [Online]. Available: http://www.megasolarsystems.com/enlightenment.php. [Accessed: 24-Mar-2016].

[10] R. Tanaka and H. Zenkoh, "Encapsulant effect on PID durability of various crystalline PV cells," *Nrel - Pvmrw 2015*, no. February, pp. 24–27, 2015.

[11] Wikipedia, "Photovoltaic system." [Online]. Available: https://en.wikipedia.org/wiki/Photovoltaic_system. [Accessed: 12-May-2016].

[12] Wikipedia, "Solar Inverter." [Online]. Available: https://en.wikipedia.org/wiki/Solar_inverter. [Accessed: 05-Jun-2016].

[13] vreg, "Evolutie van het aantal zonnepanelen en hun vermogen," Flanders, 2016.

[14] A. Ndiaye, A. Charki, A. Kobi, C. M. F. Kébé, P. a. Ndiaye, and V. Sambou, "Degradations of silicon photovoltaic modules: A literature review," *Sol. Energy*, vol. 96, pp. 140–151, Oct. 2013.

[15] R. Arndt and R. Puto, "Basic understanding of IEC standard testing for photovoltaic panels," *... [2012]. Http//Tuvamerica. Com/Services/Photovoltaics/ ...*, no. 978, pp. 1–15, 2010.

[16] M. A. Munoz, M. C. Alonso-García, N. Vela, and F. Chenlo, "Early degradation of silicon PV modules and guaranty conditions," *Sol. Energy*, vol. 85, no. 9, pp. 2264–2274, Sep. 2011.

[17] J. Schlothauer, S. Jungwirth, M. Köhl, and B. Röder, "Degradation of the encapsulant polymer in outdoor weathered photovoltaic modules: Spatially resolved inspection of EVA ageing by fluorescence and correlation to electroluminescence," *Sol. Energy Mater. Sol. Cells*, vol. 102, pp. 75–85, Jul. 2012.

[18] M. Köntges, I. Kunze, S. Kajari-Schröder, X. Breitenmoser, and B. Bjørneklett, "The risk of power loss in crystalline silicon based photovoltaic modules due to micro-cracks," *Sol. Energy Mater. Sol. Cells*, vol. 95, no. 4, pp. 1131–1137, Apr. 2011.

[19] M. Köntges, S. Kurtz, C. Packard, U. Jahn, K. A. Berger, K. Kato, T. Friesen, H. Liu, and M. Van Iseghem, "Review of Failures of Photovoltaic Modules," 2014.

[20] B. Stegemann, P. Grunow, S. Koch, M. Hanusch, S. Wendlandt, A. Böttcher, M. Roericht, and J.

Berghold, “Electrochemical Corrosion within Solar Panels,” *27th Eur. Photovolt. Sol. Energy Conf. Exhib.*, pp. 3511–3517, Oct. 2012.

[21] S. Koch, C. Seidel, P. Grunow, S. Krauter, and M. Schoppa, “Polarization effects and test for crystalline silicon cells,” *Photovoltaik Institut Berlin*, 2011. [Online]. Available: http://www.pi-solar.com/images/pdf/publication/eu_pvsec-2011-Koch_et_al-polarisation_effecs_and_test_for_crystalline_silicon_cells.pdf. [Accessed: 31-Aug-2015].

[22] P. Hacke, “Considerations for a Standardized Test for Potential-Induced Degradation of Crystalline Silicon PV Modules.” [Online]. Available: http://www.nrel.gov/docs/fy12osti/54581.pdf. [Accessed: 30-Aug-2015].

[23] V. Naumann, “PID-shunting: Understanding from nanoscale to module level,” 2014.

[24] V. Naumann, “Pid tester for solar cells,” pp. 2–3.

[25] P. Hacke, K. Terwilliger, R. Smith, S. Glick, J. Pankow, M. Kempe, and S. Kurtz, “Testing modules for potential-induced degradation,” 2014. [Online]. Available: http://www.nrel.gov/docs/fy14osti/61517.pdf. [Accessed: 31-Aug-2015].

[26] S. Hoffmann and M. Koehl, “Effect of humidity and temperature on the potential-induced degradation,” *Prog. Photovoltaics Res. Appl.*, vol. 22, no. 2, pp. 173–179, Feb. 2014.

[27] G. S. Kinsey, “Dynamic mechanical load testing,” *October 21, 2013*, 2013. .

[28] N. Bosco, T. J. Silverman, J. Wohlgemuth, S. Kurtz, M. Inoue, K. Sakurai, T. Shioda, H. Zenkoh, K. Hirota, M. Miyashita, T. Tadanori, and S. Suzuki, “Evaluation of Dynamic Mechanical Loading as an accelerated test method for ribbon fatigue,” *Conference Record of the IEEE Photovoltaic Specialists Conference*, 2013. .

[29] “Part II – Photovoltaic Cell I-V Characterization Theory and LabVIEW Analysis Code - National Instruments,” 2012. [Online]. Available: http://www.ni.com/white-paper/7230/en/. [Accessed: 19-Oct-2015].

[30] D. Pysch, A. Mette, and S. W. Glunz, “A review and comparison of different methods to determine the series resistance of solar cells,” *Sol. Energy Mater. Sol. Cells*, vol. 91, no. 18, pp. 1698–1706, Nov. 2007.

[31] D. Veldman, I. J. Bennett, B. Brockholz, and P. C. de Jong, “Non-destructive testing of crystalline silicon photovoltaic back-contact modules,” *Energy Procedia*, vol. 8, pp. 377–383, 2011.

[32] S. Brand, P. Czurratis, P. Hoffrogge, D. Temple, D. Malta, J. Reed, and M. Petzold, “Extending acoustic microscopy for comprehensive failure analysis applications,” *J. Mater. Sci. Mater. Electron.*, vol. 22, no. 10, pp. 1580–1593, 2011.

[33] Keithley Instruments, *Keithley Model 6517A Electrometer User ’ s Manual*. 1996.

[34] Institute of precision engineering, “Keithley 6517A.” [Online]. Available: http://www.ipe.cuhk.edu.hk/Equipment_list/Electrometer.htm. [Accessed: 05-Jun-2016].

[35] Keithley Instruments, “Model 228A.”

[36] EEVblog Electronics Community Forum, “Which electronic DC load to choose?” [Online]. Available: http://www.eevblog.com/forum/testgear/which-electronic-dc-load-to-choose/. [Accessed: 05-Jun-2016].

[37] Weiss Technik, *Installatie handleiding en gebruiksaanwijzing Klimaattestkast Type: SB22/160/80*. 1998.

[38] Logitech, “HD Webcam C310.” [Online]. Available: http://www.logitech.com/nl-be/product/hd-webcam-c310?crid=34. [Accessed: 25-Mar-2016].

[39] Oriel Instruments, “e-Catalog Newport 91150V.” [Online]. Available: http://www.nxtbook.com/nxtbooks/newportcorp/resource2011/#/86. [Accessed: 25-Mar-

2016].

[40] Newport, “Calibrated reference cell and meter, quartz windon.” [Online]. Available: https://www.newport.com/p/91150V. [Accessed: 05-May-2016].

[41] Avantes, “AvaSpec-3648 Fiber Optic Spectrometer.” [Online]. Available: http://www.wacolab.com/avantes/spectrometers14.pdf. [Accessed: 28-Apr-2016].

[42] Wikipedia, “LabVIEW.” .

[43] Wikipedia, “Autodesk Inventor.” .

[44] Edulearn, “What is Autodesk Inventor?” [Online]. Available: http://www.edulearn.com/article/what_is_autodesk_inventor.html. [Accessed: 12-May-2016].

[45] FESTO, “Swivel modules DSM / DSM-B.” p. 58.

[46] E. Dunlop, F. Fabero, G. Friesen, W. Herrmann, J. Hohl-Ebinger, H.-D. Mohring, H. Müllejans, A. Virtuani, W. Warta, W. Zaaiman, and S. Zamini, “Guidelines for PV Power Measurement in Industry,” 2010.

[47] Newport, “Oriel Sol3A Class AAA Solar Simulators.” [Online]. Available: http://www.newport.com/Oriel-Sol3A-Class-AAA-Solar-Simulators/842468/1033/info.aspx. [Accessed: 28-Apr-2016].

Auteursrechtelijke overeenkomst

Ik/wij verlenen het wereldwijde auteursrecht voor de ingediende eindverhandeling:
Detection and acceleration of potential induced degradation on silicon photovoltaic modules

Richting: **master in de industriële wetenschappen: energie-elektrotechniek**
Jaar: **2016**

in alle mogelijke mediaformaten, - bestaande en in de toekomst te ontwikkelen - , aan de Universiteit Hasselt.

Niet tegenstaand deze toekenning van het auteursrecht aan de Universiteit Hasselt behoud ik als auteur het recht om de eindverhandeling, - in zijn geheel of gedeeltelijk -, vrij te reproduceren, (her)publiceren of distribueren zonder de toelating te moeten verkrijgen van de Universiteit Hasselt.

Ik bevestig dat de eindverhandeling mijn origineel werk is, en dat ik het recht heb om de rechten te verlenen die in deze overeenkomst worden beschreven. Ik verklaar tevens dat de eindverhandeling, naar mijn weten, het auteursrecht van anderen niet overtreedt.

Ik verklaar tevens dat ik voor het materiaal in de eindverhandeling dat beschermd wordt door het auteursrecht, de nodige toelatingen heb verkregen zodat ik deze ook aan de Universiteit Hasselt kan overdragen en dat dit duidelijk in de tekst en inhoud van de eindverhandeling werd genotificeerd.

Universiteit Hasselt zal mij als auteur(s) van de eindverhandeling identificeren en zal geen wijzigingen aanbrengen aan de eindverhandeling, uitgezonderd deze toegelaten door deze overeenkomst.

Voor akkoord,

Coppieters, Jordy

Datum: **6/06/2016**